Quantum suppression of superconductivity in nanowires

2008 J. Phys.: Condens. Matter 20 043202

(http://iopscience.iop.org/0953-8984/20/4/043202)

IOP PUBLISHING JOURNAL OF PHYSICS: CONDENSED MATTER

J. Phys.: Condens. Matter **20** (2008) 043202 (19pp) doi:10.1088/0953-8984/20/04/043202

TOPICAL REVIEW

Quantum suppression of superconductivity in nanowires

Alexey Bezryadin

University of Illinois at Urbana-Champaign, Urbana, IL, USA

Received 6 October 2007, in final form 7 November 2007
Published 8 January 2008
Online at stacks.iop.org/JPhysCM/20/043202

Abstract

It is of fundamental importance to establish whether there is a limit to how thin a superconducting wire can be, while retaining its superconducting character—and if there is such limit, to understand what determines it. This issue may be of practical importance in defining the limit to miniaturization of superconducting electronic circuits. Recently, a new fabrication method, called molecular templating, was developed and used to answer such questions. In this approach, a suspended carbon nanotube is coated with a thin superconducting metal film, thus forming a superconducting nanowire. The wire obtained is automatically attached to the two leads formed by the sides of the trench. The usual material for such wires is the amorphous alloy of MoGe (Graybeal 1985 *PhD Thesis* Stanford University; Graybeal and Beasley 1984 *Phys. Rev.* B **29** 4167; Yazdani and Kapitulnik 1995 *Phys. Rev. Lett.* **74** 3037; Turneaure *et al* 2000 *Phys. Rev. Lett.* **84** 987). Such wires typically exhibit a high degree of homogeneity and can be made very small: as thin as ∼5 nm in diameter and as short as ∼40 nm in length. The results of transport measurements on such homogeneous wires can be summarized as follows. Short wires, shorter than some empirical length, ∼200 nm for MoGe, exhibit a clear dichotomy. They show either a superconducting behavior, with the resistance controlled by thermal fluctuations, or a weakly insulating behavior, with the resistance controlled by the weak Coulomb blockade. Thus a quantum superconductor–insulator transition (SIT) is indicated. Longer wires exhibit a gradual crossover behavior, from almost perfectly superconducting to normal or weakly insulating behavior, as their diameter is reduced. Measurements of wires, which are made inhomogeneous (granular) on purpose, show that such wires, even if they are short in the sense stated above, do not show a clear dichotomy, which could be identified as an SIT (Bollinger *et al* 2004 *Phys. Rev.* B **69** 180503(R)). Thus, inhomogeneity destroys the SIT, as in the case of thin superconducting films (Frydman 2003 *Physica* C **391** 189–95). Here, only properties of homogeneous wires are reviewed.

1. Introduction

Thin superconducting nanowires have properties in many ways similar to so-called 'weak superconducting links' [7]. Nanowires have been used as detectors and mixers of microwave radiation [8–10]. Superconducting nanowires can find applications in classical [11, 12] and possibly quantum information-processing devices. Quantum devices are those which exhibit a macroscopic quantum behavior. A program to study macroscopic quantum phenomena was initiated by Leggett around 1980 [13–17]. A ultimate experimental demonstration that a macroscopic object can behave as a single quantum particle was given by Martinis, Devoret, and Clarke in 1987 [18]. They used a microwave technique and showed that a micron-size superconducting device possesses a discrete energy spectrum. In addition, they showed that the device is capable of macroscopic quantum tunneling (MQT), i.e. that it can be in a quantum superposition of macroscopically distinct states. Macroscopic quantum devices can be used as qubits in quantum computers [19–22]. Superconducting qubits based on nanowires were recently proposed by Mooij, Harmans, and Nazarov [23, 24]. The problem of MQT in quasi-one-dimensional (1D) superconducting systems, such as

thin superconducting wires, remains an active field of research today, with many questions unanswered [25–35].

A distinctive property of thin superconducting wires is that, due to thermal fluctuations, the resistance of a quasi-1D nanowire remains greater than zero at any finite temperature below its critical temperature T_C [36–41]. The basic reason for this is that at any finite temperature each segment of a thin wire has a non-zero probability of becoming normal for a short period of time (typically $\sim 10^{-11}$–10^{-12} s). Typical dimensions of such fluctuations are of the order of the coherence length. Since the wire diameter is assumed smaller than the coherence length, it is clear that each such fluctuation should disrupt the flow of supercurrent and thereby impart a non-zero resistance to the wire. Such fluctuations are called thermally activated phase slips (TAPS). The superconducting phase along the wire 'slips' by 2π each time a normal region appears in the wire. The TAPS are strongly pronounced only very near T_C, unless the wire is very thin. The resistance of the wire is linearly proportional to the rate of TAPS. As the temperature is lowered, their rate exhibits a fast drop, following the Arrhenius law. Thus TAPS cause a broadening of the apparent superconducting transition of the wire. For example, for a MoGe wire of diameter $\sim$10 nm, the apparent resistive transition region width is typically of the order of 1 K, while for a Sn wire of the order of 1 μm in diameter the transition region might be as narrow as $\sim$1 mK [41]. Yet, strictly speaking, the resistance of a wire is never exactly zero, due to the fact that TAPS has a nonzero probability at any finite temperature, but it can be exponentially low.

In principle, a wire can fall into one of the following three different categories: (i) 'truly superconducting', i.e. approaching zero resistance ($R = 0$) in the limit of zero temperature ($T = 0$), as the TAPS freeze out, (ii) 'resistive' or 'normal', with $R > 0$ at $T = 0$ (such situation might occur due to tunneling of quantum phase slips (QPS)), and (iii) insulating, with $R \to \infty$ as $T \to 0$. Intuitively, it seems natural to expect that, at some point, thin wires should lose their superconducting qualities as the diameter is gradually reduced, approaching zero. Assuming this is true, and assume also that wires thicker than a certain limit are truly superconducting, then one can expect one or more quantum transitions, associated with destruction of superconductivity, to occur as the wire diameter is reduced, at zero temperature. Such transitions are usually called superconductor–insulator transitions (SIT). General conditions under which SIT(s) happen are not well established, although, as we shall demonstrate, there is much evidence, experimental as well as theoretical, indicating that such transitions do exist.

The existence of an SIT implies the existence of at least two distinct regimes, namely a superconducting regime (with $R \to 0$ as $T \to 0$) and an insulating regime (with $R \to \infty$ as $T \to 0$). Results supporting the SIT scenario, namely the observations of two qualitatively different families of $R(T)$ curves, usually with the resistance decreasing with cooling in thicker wires and the resistance increasing with cooling in thinner wires, have been reported, for example, in [42, 34, 25, 26, 5]. A number of SIT theories have been suggested already, including Berezinskii–Kosterlitz–Thouless type quantum transition, generalized for QPS [28], and theories depending on a quantum dissipative environment [43–45], similar to the Schmid–Bulgadaev (SB) [46] transition [47–51], which was observed experimentally on resistively shunted Josephson junctions [52, 35]. Recent experiments on short wires ($L < 200$ nm) suggest that the total wire resistance in the normal state R_N is a better control parameter compared to the wire diameter d [53]. An approximate and simple rule was found empirically: the resistance of wires with $R_N < R_Q \equiv h/4e^2 \approx 6.45$ kΩ decreases exponentially with cooling, while wires with $R_N > R_Q$ shows a weakly insulating behavior. This behavior suggests that an SIT takes place. The fact that the apparent critical point is given by the condition $R_N \approx R_Q$ suggests that the observed SIT may be of a similar origin as the SB transition, although an important difference is present: the nanowires were measured without any external shunting resistor present. But, some sort of self-shunting might be occurring, due to a collective effect of multiple QPS normal cores, as was suggested by Bollinger *et al* [54]. A renormalization theory that includes collective QPS effects was developed by Meidan *et al* [45]. Another, different but important fact is that the homogeneity of samples appears to be a necessary requirement for the observation of an SIT[1].

On the other hand, many results were published during recent years that can be understood as providing evidence against the occurrence of any SIT in thin wires. These results imply that the rate of quantum phase slips is higher than zero for a wire of any diameter. In other words, any wire is characterized by $R \to R_0 > 0$ as $T \to 0$ (although R_0 is expected to drop very rapidly with increasing diameter). So, the wire is always 'normal' or 'resistive', and there are no distinct phases. A large number of experimental and theoretical results [25, 27, 55–57] assume such a gradual crossover. Experimentally, the presence of QPS is usually concluded if a resistive 'tail' is observed. In other words, if the measured resistance exceeds the one expected from the TAPS model. It should be noted, nevertheless, that other effects have been suggested to cause additional (compared to pure TAPS) broadening of the resistive transition. Such explanations include 1D Coulomb correlation effects [42] and various inhomogeneities of the wires [5, 58].

2. Molecular templating fabrication method

A technique of molecular templating (MT) can be used to fabricate thin and short metallic wires with ultrasmall dimensions. The technique [26] employs a suspended linear molecule as a template subjected to a metal deposition process

[1] A well defined superconductor–insulator transition can only be observed on a family of homogeneous wires [5]. Inhomogeneous wires typically show multiple resistive transitions and multiple critical-current-like peaks in the differential resistance versus current curves, $dV(I)/dI$. Their $R(T)$ curves frequently show 'tails', somewhat similar to the QPS 'tails'. As their diameter is reduced, they show an ill-defined crossover from a predominantly superconducting to a predominantly insulating behavior. Yet most of the inhomogeneous wires exhibiting a mixed behavior, with some superconducting and some insulating characteristics present in the same sample. Hence, inhomogeneous wires, usually identified by multiple steps on their $R(T)$ curves and/or multiple critical-current-like peaks on $dV(I)/dI$, are excluded from consideration in this review.

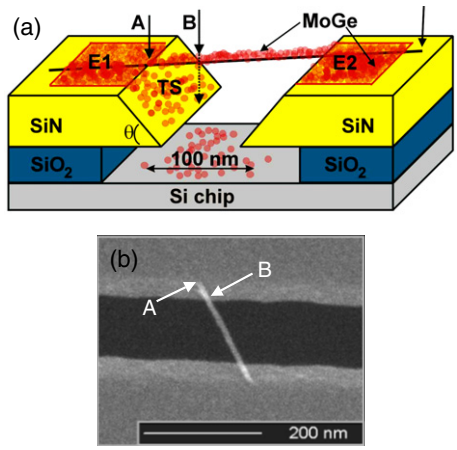

Figure 1. Molecular templating of nanowires. (a) Schematic illustration of molecular templating fabrication of thin metallic wires. A nanotube (the horizontal black line indicated by a vertical arrow on the right side) is positioned across a trench, which is etched into the top SiN layer (yellow) of thickness ∼100 nm. The underlying SiO_2 is used to create an undercut and to improve electrical insulation of the electrodes from the Si substrate. A superconducting metal (typically MoGe) is sputtered over the entire surface of the Si chip. Red circles schematically represent atoms of Mo and Ge. Since the sputtered metal sticks to the suspended nanotube, the tube transforms into a metallic nanowire, seamlessly connected to the electrodes, simultaneously deposited on the banks of the trench. Photolithography and reactive ion etching (or wet etching in H_2O_2) are subsequently employed in order to defining the shape of the electrodes (E1 and E2) and destroy all wires but the one protected with photoresist. The segment of the wire located between arrows marked A and B is suspended over the tilted sides (TS) of the trench. This segment appears brighter in SEM images and is called a 'white spot'. (b) A scanning electron micrograph (SEM) of a real nanowire suspended over a trench (black) and connecting to two MoGe electrodes (gray areas). The white spots are visible on both sides of the wire. The beginning and the end of one of the white spots is marked by arrows A and B. The presence of white spots at each end of the wire indicates its good quality. Absence of white spots indicates imperfections of the sample, such as the wire not being coplanar with the electrodes or not straight, or it is not well connected to the electrodes.

(figure 1). The molecule has to be rigid, straight, and stable enough to withstand the sputtering deposition process. The molecule should also provide a good mutual adhesion with the sputtered metal in order to avoid the grain formation. It was found empirically that materials such as MoGe and Nb [59, 60] have a good adhesion to carbon nanotubes. The amorphous MoGe alloy [1–4] is probably the best choice for making wires with nanotube templates, since it makes a homogeneous coating. MoGe is a strongly disordered alloy with a short electronic mean free path, $l \sim 3$–4 Å and a rather high superconducting critical temperature $T_C \approx 7.4$ K in bulk samples. Other metals form grains when evaporated on a nanotube. One way to improve the adhesion is to coat the molecule with a thin Ti layer [61]. The list of molecules, which were used successfully as molecular templates, includes carbon nanotubes [26, 27], fluorinated carbon nanotubes (fluorotubes) [62, 5], DNA molecules [63], and WS_2 nanorods [64]. An amorphous InO was used as a coating material in the case of WS_2 nanorods. Unlike regular nanotubes, the fluorotubes are 100% insulating and should be used when the conductivity of the supporting molecule is undesirable. It was found that MoGe wires made on insulating fluorotubes [5] have similar properties to those made on regular nanotubes [26]. Since the molecules used as templates are very thin, 1–3 nm in diameter, the resulting nanowires that can be obtained are considerably thinner than 10 nm in diameter. This fact makes the MT method unique since it is very difficult to obtain wires thinner than ∼10 nm in diameter with more traditional fabrication methods.

In MT (figure 1), the fabrication is done on a Si (100) wafer covered with a layer of 500 nm thick SiO_2, including 100 nm dry oxide and 400 nm wet oxide layers, and a 60 nm thick film of low stress SiN [65]. A narrow (∼100 nm) and long (∼5 mm) trench is then defined in the SiN film using electron beam (e-beam) lithography and reactive ion etching with SF_6 plasma. A focused ion beam can be used, if desired, instead of e-beam lithography. An undercut is then formed by wet etching in HF for ∼10 s. In a ∼50% concentrated HF-in-water solution, the undercut quickly develops, due to the fact that this acid etches silicon oxide much faster than the silicon nitride. Making the undercut is an important part of the sample fabrication: it ensures that the electrodes formed in the subsequent metal sputtering step are electrically disconnected. (More precisely, the electrodes are connected through the nanowire, but they are not connected anywhere else.)

Fluorinated nanotubes are deposited from a solution in isopropyl alcohol. If regular carbon nanotubes are used, they should be dispersed in dichloroethane. After being blown dry with a nitrogen gun, the sample is sputter coated with the desired superconducting metal, typically ∼5–15 nm of $Mo_{79}Ge_{21}$ (figure 1). After sputtering, each nanotube which is suspended over the trench becomes coated with metal to form a metallic nanowire. The metal is located mostly above the nanotube, although some amount can also diffuse under the nanotube, since sputtering is not a completely directional deposition process. In SEM, such nanowires appear continuous and homogeneous (figure 2). Some apparent surface roughness can be attributed to the amorphous morphology of the wire and to the surface oxidation, due to exposure to air. After the sputtering, one obtains many such nanowires crossing the trench.

It is important to ensure that the wire selected for measurements is straight and is coplanar with the electrodes. If the wire is not coplanar, then the film electrodes are not connected directly to the wire, but only through poorly metallized regions on the inner sides of the trench (the TS region in figure 1(a)). To ensure the nanowire straightness, only wires with so-called 'white spots', visible on the corresponding SEM images (figure 1(b)), are selected for measurements. The beginning and the end of one such white spot, at the left end of the wire, are indicated by arrows marked A and B (figure 1(b)). The reason why such white spots are visible in SEM is explained in the schematic drawing of figure 1(a). The region between the marker 'A' and marker 'B' on this schematic shows the segment of the nanotube suspended over the tilted side (TS) of the trench. Thus the SEM image includes superimposed images of the wire and

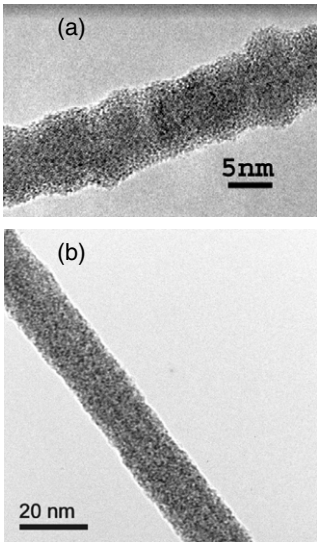

Figure 2. (a) A transmission electron micrograph (TEM), made using JEOL 2010F microscope, of one of the thinnest MoGe wire. The apparent width is ∼8 nm. Since a surface layer of about 2–3 nm is oxidized [5], the actual width of the conducting core of this wire can be estimated ∼4 nm. Some surface oxide is indeed visible in the image. It appears as a material of somewhat different morphology and brightness compared to the material in the middle of the wire. The nanowire on this micrograph was made by sputter deposition of a 7 nm thick $Mo_{79}Ge_{21}$ film over the surface of a fluorinated nanotube. The nanotube itself is not visible since it is coated by the alloy. This sample was prepared on a TEM substrate with small holes, specifically for making such images. (b) Another example of a typical MoGe wire with a larger diameter [66].

the side of the trench right under it. Together, they produce the appearance of a brighter region. In the cases when the nanotube is not straight, but, rather, it tilts down the trench and cross the gap at the level of the bottom surface of the SiN film (i.e. ∼100 nm below the plane of the film electrodes), such white spots do not appear. Thus, wires which have no white spots are considered not straight and they should not be selected for transport experiments. As is clear from figure 1(a), white spots can only occur if the trench side slope is $\theta < 90°$, which is usually the case. The trench side slope is caused by the isotropic nature of the SF_6 reactive ion etch that created the trench. In practice, such white spots are only observed for trenches which are narrower than about 200 or 300 nm. On trenches wider than this, the templating nanotube almost always sticks to the sides of the trench (the 'TS' region in figure 1(a)), tilts down the trench, and crosses the trench at the level of the bottom surface of the SiN layer. For this reason white spots do not occur. The resulting nanowire is not directly connected to the leads, but only through the 'TS' region (figure 1(a)), which may not be well metallized and can act as a weak link. This might explain the fact that the majority of wires longer than ∼200–300 nm, made by the MT method outlined here, appear as inhomogeneous wires in transport measurements. Namely, they typically exhibit multiple resistive transitions, resistive tails and multiple critical currents.

After a desired wire is chosen, photolithography, guided by a set of markers positioned along the trench (not shown), is employed in order to pattern the electrodes (figure 1(a)) and for etching away of all nanowires except the selected one. Unlike in the schematic drawing of figure 1(a), in a practical device the number of contact pads has to be at least four, but usually the number is five [26], to allow 4-probe measurements on the wire. A ready Si chip is then installed into a plastic chip carrier with nonmagnetic metallic pins. The connection of the samples electrodes to the pins is done using gold wires and indium dots. The person making the connections is always grounded, in order to prevent burning of the wire with static electricity.

3. Transport measurements of nanowires

In what follows we describe a set-up used to observe an SIT on short wires [5, 53, 66]. Transport experiments, which include zero-bias resistance versus temperature $R(T)$, voltage versus bias current $V(I)$, and the differential resistance versus bias current $\mathrm{d}V(I)/\mathrm{d}I$ measurements, are typically done in a He-3 cryostat equipped with RF-filtered leads. In order to measure $V(I)$ curves, a sinusoidal AC current (at 12.7 Hz frequency and 1–10 nA amplitude) is injected through the superconducting thin film electrodes. The voltage is measured using a separate pair of leads also connected to the thin film electrodes [26, 66]. The measurement is done with a low noise battery-operated preamplifier, namely PAR 113 or SR560. The current is taken from a high precision function generator (Stanford Research Systems, DS 360), connected to the sample through a standard 1 MΩ series resistor, which defines the current value. The voltage on the standard resistor is measured with another PAR 113 (or SR560) preamplifier. The bias current is then calculated using the known, fixed value of the series resistor. The zero-bias, i.e. 'linear', resistance of the sample is determined from the slope of the best linear fit to the $V(I)$ curves measured at a low driving current (∼3 nA), with the DC component of the bias current being zero. The bias current amplitude is chosen small enough in order to assure linear response conditions. The temperature is measured using a commercially calibrated ruthenium oxide thermometer (from *Lake Shore Cryotronics, Inc.*). The leads connecting the sample are made of a Teflon-coated resistive alloy wire, *Stablohm 800*, produced by California Fine Wire Co. Before reaching the sample, these 1 m long Stablohm wire leads are rolled over a cold Cu rod (the Cu rod is rigidly connected to the He-3 pot of the refrigerator) and coated with a layer of a conducting silver paste. This coating with such electrically and thermally conducting glue ensures that the leads are cooled to the base temperature and RF filtered. Note that the sample itself is cooled through the measurement leads. The coating of the signal wires with the silver paste also acts as a microwave radiation filter. It prevents the room temperature black body radiation from impacting the sample. Similar filters are frequently made with Cu powder coating and are known as 'Cu powder filters'. They were used by the Clarke group in their classic experiments in which macroscopic quantum tunneling was demonstrated [18]. All electrical signal lines reaching the sample or the thermometer, positioned in close proximity to

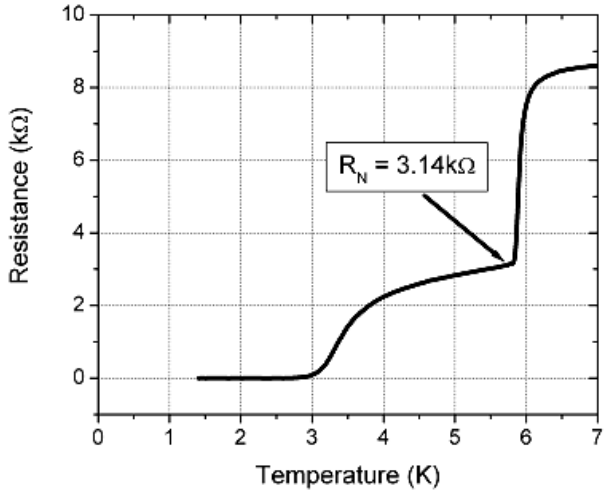

Figure 3. A typical resistance versus temperature curve for a MoGe nanowire sample. The higher temperature resistance drop corresponds to the superconducting transition in the thin film electrodes adjacent to the wire. The second, broader transition reflects the establishment of superconductivity in the wire. The normal state resistance R_N of the wire is defined at a temperature that is slightly lower than the critical temperature of the electrodes, as is shown by the arrow. The width of the film transition is ∼0.2 K and the apparent width of the wire transition is ∼1 K, which is its intrinsic property and is due to its small diameter and the corresponding low barrier for phase slips.

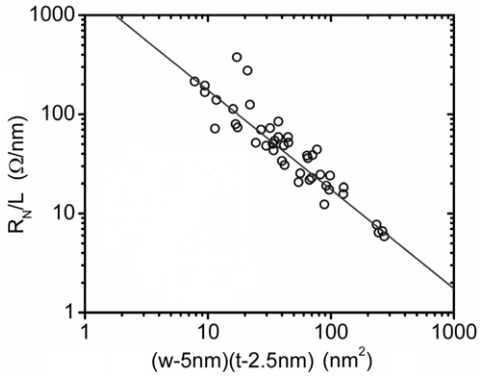

Figure 4. The normal state resistance, divided by the wire length, is plotted (open circles) versus the wire cross sectional area, for a set of 23 superconducting wires, 14 insulating wires and 7 'mixed' wires. (All of such mixed wires were long wires, with $L \sim 500$ nm. The mixed behaviour is typically observed in inhomogenous wires [5]. Long wires frequently turned out inhomogenous, at least slightly.) [66]. The effect of oxidation has been taken into account by subtraction appropriate values from the width w and the thickness of the wire t, as is discussed in the text. The line represents the fit $R_N/L = \rho/[(w - 5\text{ nm})(t - 2.5\text{ nm})]$, where the resistivity that gives the best fit is $\rho = 175\ \mu\Omega$ cm. The subtraction of 5 nm from the measured width and 2.5 nm from the nominal sputtered thickness is done in order to account for the approximate 2.5 nm surface layer of MoGe being oxidized on each side of the wire as well as on its top surface, due to air exposure.

the sample, are also filtered on the top of the cryostat with π-filters [67]. All measurements on thin wires are performed under the condition that only electrically 'quiet' equipment is allowed to be directly connected to the sample. In other words, only preamps which do not impose any excessive voltage or current noise on the sample can be used. On the other hand, some of the more traditional precision instruments, such as certain types of digital voltmeters for example, may generate high frequency (10–100 kHz) voltage spikes, up to ∼100 mV in amplitude, even on their input terminals. Such voltage or current noise, if it reaches the sample, can induce additional phase slips in the nanowire and can make the wire to appear more resistive than it actually is. A device like this should not be directly plugged to the signal leads connected to the sample. Incorrect grounding of the set-up can also cause resistive tails, similar to those typically described as QPS-related resistive tails.

A typical $R(T)$ curve is shown in figure 3. Since the wire is connected in series with the thin film electrodes, two resistive transitions are observed. The first one (at ∼6 K) is due to the electrodes becoming superconducting. This fact was confirmed by independent measurements of thin film electrodes connected to the wire [26]. The second transition (at ∼3.5 K) is due to the nanowire losing its resistance. Wires made of MoGe alloy always show a lower critical temperature than films of the same thickness. We define the normal state resistance of the wire, R_N, as the sample resistance measured immediately below the temperature at which the leads become superconducting, as is shown by an arrow in figure 3.

4. Resistivity of metallic nanowires

Resistivity of nanowires is difficult to determine accurately since it is difficult to measure precisely the cross section area of the conducting core of the wire. The width of the wire w, measured with SEM, is larger by a few nanometers than the width of the conducting core of the wire, due to the surface oxidation and some smearing of the SEM images at the scale of a few nanometers. Transport properties of wires made on TEM-compatible substrates have not been studied so far. An analysis of a large set of wires with the goal of confirming their homogeneity was done by Bollinger [66], as is reproduced in figure 4. The vertical axis is the normal resistance of the wires divided by its length, measured under the SEM (Hitachi S-4700 High Resolution SEM). The horizontal axis (figure 4) includes a product of the wire thickness t, which is taken to be equal to the nominal thickness of the sputtered MoGe and the wire width w, measured under the SEM. In this approximate model the wire cross section is assumed to be a rectangle with dimensions w and t. The actual metallic core of the wire is smaller than these dimensions due to the surface oxidation. The effect of oxidation has been taken into account by reducing the width w and the thickness t by independently estimate [5] oxidized thickness values of 5 and 2.5 nm, respectively. Note that the width is reduced by twice the usual oxidation layer thickness, due to the fact that both sides of the wire are oxidized. The horizontal axis in figure 4 is chosen as a product of the oxidation-corrected width and oxidation-corrected thickness, namely as $(w - 5\text{ nm})(t - 2.5\text{ nm})$. A fit of the form $R_N/L = \rho/[(w-5\text{ nm})(t-2.5\text{ nm})]$ is also shown in figure 4. It appears as a straight line, since

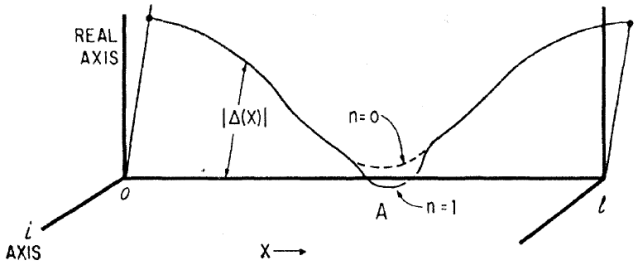

Figure 5. Original Little's phase slip diagram [36]. The complex superconducting order parameter of a thin wire ring is drawn as a function of the position along the ring. Two possible configurations are shown, one is for an order parameter in the sub-ensemble $n = 0$ (no vortices present in the ring) and the other one is for $n = 1$ (one vortex present in the ring). Near the point A, $\psi_1(x)$ makes an excursion around zero on the Argand plane, while $\psi_0(x)$ does not. The transition from $n = 0$ to 1 constitutes a phase slip event. This transition can be viewed as a vortex, with its normal core, passing across the wire. Hence, the transition between the $n = 0$ and 1 states can only occur if the order parameter reaches zero somewhere on the wire.

the graph is formatted as a log–log plot. The best-fit slope gives the resistivity $\rho = 175\ \mu\Omega$ cm, in agreement with previously published values of resistivity for bulk MoGe and thin film MoGe [1]. This type of fit is done in order to verify that all wires are characterized by the same bulk resistivity of MoGe. The graph (figure 4) includes both types of samples: superconducting as well as insulating samples. This plot shows that normal state properties of the insulating wires and the superconducting ones are not significantly different. Thus, it is possible to rule out a trivial explanation for the observed SIT, namely that superconducting wires behave superconducting since they are homogeneous and insulating wires behave insulating since they become granular due to the fact that they are thinner. If that were the case, these two types of wires would necessarily form two distinct families on the plot of figure 4, with different values of the corresponding resistivity. It is clearly not the case, as samples tend to follow the same best fit, i.e. the straight line in figure 4.

5. Little's phase slip

The notion of a phase slip was introduced by William Little in 1967 [68]. This theory was developed in order to understand the mechanism of the supercurrent decay in thin wires and to justify Little's earlier proposal of a superconducting macromolecule [69]. Following Ferrell [70] and Rice [71], Little's argument is based on the assumption that the superconducting order parameter is defined locally (as well as globally) in a thin wire. The local amplitude of the order parameter is subject to thermal fluctuations. Each time a fluctuation strong enough to reduce the order parameter to zero happens at some point along the wire, the 'order parameter spiral' (figure 5), representing a supercurrent in the wire, is able to unwind. Thus a dissipation of supercurrent occurs and the wire gains a non-zero electrical resistance. This resistance is defined by an Arrhenius type equation with a temperature-dependent energy barrier, which is determined by the condensation energy required to locally suppress the order parameter to zero. The minimum energy barrier (the 'saddle' point) corresponds to fluctuations in which the order parameter is suppressed in wire segments with lengths on the order of the coherence length $\xi(T)$.[2] The occurrence of TAPS causes nanowires to remain resistive at any nonzero temperature, although the resistance drops exponentially with cooling. This property is in agreement with the general rule that no thermodynamic phase transition can occur in a one-dimensional (1D) system [39, 70–72]. A more precise calculation of the energy barrier for phase slips was given by Langer and Ambegaokar (LA) [73], and the attempt frequency was derived by McCumber and Halperin (MH) [74]. Therefore the TAPS theory is also known as the LAMH theory. The calculations were based on the Ginzburg–Landau (GL) theory, which is valid only very near T_C, with the exception [75] of samples having a short mean free path (i.e. dirty superconductors), which is the case for MoGe. The MH calculation, based in time-dependent G–L theory, is not exactly applicable to the tested wires, since the superconductivity in them is not gapless, but it gives a useful approximation.

Early experiments on 0.5 μm diameter tin whiskers, by Lukens *et al* and Newbower *et al*, confirmed the LAMH theory [41, 76]. In [41], in order to improve the fit to the data, quasiparticle conductance near T_C was included in parallel with the conductance of the condensate. Recently, a structure of TAPS in a clean, one-dimensional superconductor, in which superconductivity occurs only within one or several identical conducting channels, was developed by Zharov *et al* [77]. An exact analytical solution in the whole temperature and current range was found. Another recent development, by Pekker *et al*, is a generalization of the LAMH theory to include two-wire devices and the corresponding interference in magnetic fields [78].

Little's idea of a phase slip is illustrated in figure 5. Although the original analysis was applied to the understanding of a supercurrent stability in a closed loop (ring), made of a thin wire, the same analysis is in fact applicable to the understanding of the decay of the supercurrent flowing in a straight wire connected to leads. In this graph (figure 5), the complex order parameter $\psi = |\psi(x)|e^{i\varphi(x)}$ of a thin wire ring is plotted as a function of the position along the ring x. Two possible configurations are shown (ψ_0 and ψ_1), the first one is for an order parameter in the sub-ensemble $n = 0$ (no vortices present in the ring) and the other one is for $n = 1$ (one vortex present in the ring). Under a 'vortex' we understand such a configuration of the complex order parameter for which the phase changes by 2π as the point of observation circles the wire loop once. On figure 5, near the point A, ψ_1 makes an excursion around zero on the Argand plane, while ψ_0 does not make such excursion. Although the apparent difference between these two curves is small and local, it is, in fact, very significant. Specifically, the state ψ_1 corresponds to a phase difference of 2π along the ring and, as a result, carries some nonzero supercurrent. The state ψ_0, on the other hand, corresponds to zero

[2] A superconducting nanowire behaves as one-dimensional (1D) if its diameter is smaller than about $4.4\xi(T)$. See figure 12 in [7].

phase difference and, correspondingly, zero net supercurrent. The transition from ψ_1 to ψ_0 constitutes a phase slip event that topologically requires the order parameter curve to cross the x-axis in the diagram, i.e. requires the condition $\psi = 0$ to be satisfied at some time somewhere along the wire. In other words, a phase slip is an event analogous to a vortex normal core passing across the wire.

In each phase slip event the phase difference between the ends of the wire can only change by an integer multiple of 2π. Such slippage by $2\pi n$ (n is an integer), unlike a phase change by any other value, does not require a voltage to be applied to the leads, since their phases are defined modulo 2π. The phase difference between the leads is defined by the number of times the order parameter goes around zero on the Argand plane as the point of observation moves along the wire. So as this number of phase revolutions is reduced by one loop, the phase difference is reduced by 2π.

A finite resistance occurs at constant voltage bias, in the following way. The voltage applied to the ends of the wire increases the phase difference between the ends of the wire and thus tends to increase the supercurrent. At the same time the phase slips occurring stochastically at all points along the wire tend to unwind the phase and to reduce the supercurrent. A dynamic equilibrium is established at a supercurrent value that is linearly dependent on the applied voltage (for small voltages). Thus a finite resistance occurs. Two different approaches to calculating this resistance are presented below: the Little's fit and the LAMH model.

6. Little's fit

Probably the simplest approximation one can think of that describes the resistance of a nanowire, at temperatures below its mean-field critical temperature T_C, is the 'Little's fit':

$$R(T) = R_N \exp(-\Delta F/k_B T). \quad (1)$$

Equation (1) is based on the Arrhenius law. Here k_B is the Boltzmann constant, T is the temperature, ΔF is the barrier for phase slips, which depends on temperature and goes to zero at $T = T_C$. At temperatures close to T_C this formula is not accurate since it gives $R(T_C) = R_N$; the actual wire resistance should be less than R_N, due to superconducting fluctuations. Nevertheless, equation (1) describes the resistive transition in bridges [79] and nanowires [80] quite well at low temperatures, at which the Arrhenius factor changes much faster than the pre-exponential factor, so that making this pre-factor a constant does not change much the overall shape of the $R(T)$ dependence. To practically use this formula (equation (1)) one needs to know the energy barrier ΔF as a function of temperature. A phase slip requires a complete suppression of superconductivity in some volume. The energy barrier is the lowest in the case when the length of the volume where the order parameter is suppressed equals the GL coherence length $\xi(T)$. Such choice of the phase slip length minimizes both the amplitude and the gradient terms of the condensate free energy [81]. The cross sectional area of the volume is equal to the cross sectional area of the wire A, provided that the wire diameter is smaller or about equal to the coherence length. So the energy barrier can be estimated as a product of the effective volume of a phase slip $\sim \xi(T)A$ and the condensation energy density $H_C^2/8\pi$, namely $\Delta F(T) \sim \xi(T)A[H_C^2(T)/8\pi] \sim (1 - T/T_C)^{3/2}$. Here, the usual temperature-dependent expressions for the critical field $H_C(T) = H_C(0)(1 - T/T_C)$ and the coherence length $\xi(T) = \xi(0)/\sqrt{(1 - T/T_C)}$ are used. At low temperatures the following empirical form of the temperature dependence is more accurate $H_C(T) \propto (1 - (T/T_C)^2)$ though, as was illustrated in [54]. A more exact calculation of the free energy barrier is based on the following exact form of the order parameter $|\psi| = \psi_0 \tanh[(x - x_0)/2\xi(t)]$. This is a solution of the Ginzburg–Landau equation, which has a single point $x = x_0$ at which the order parameter is zero [81]. This solution gives the shape of the phase slip, but only at zero-bias current [37]. The Ginzburg–Landau free energy of this solution, referenced to the constant order parameter free energy, is $\Delta F(T) \approx (8\sqrt{2}/3)A\xi(0)[H_C^2(0)/8\pi](1 - T/T_C)^{3/2}$ [37], and it is exactly valid only near the critical temperature, as far as the approximation $H_C(T) \propto (1 - T/T_C)$ is valid.

To plot a Little's fits, one needs to use two fitting parameters, the wire critical T_C and the product $A\xi(0)H_C^2(0)$. Or, in the Tinkham and Lau formulation [82], the barrier can be expressed as $\Delta F(T) = 0.83 k_B T_C (R_Q/R_N)(L/\xi(0))(1 - T/T_C)^{3/2}$. The normal resistance can be determined from a high temperature measurement and the wire length can be directly measured under SEM. The T_C of MoGe wires is size dependent and usually not known exactly for a given wire. The same is true for the coherence length $\xi(0)$. Thus these two quantities are used as free fitting parameters. Another, similar approach is to use the critical current of the wire as an adjustable parameter, instead of the coherence length. The corresponding barrier height is $\Delta F(T) = \sqrt{6}(\hbar/2e) I_C(T)$ [82].

A simple 'derivation' of equation (1) can be given following the hypothesis stated by Little [36]: 'We can therefore calculate the time average of the resistance ... by determining what fraction of the time some part of the loop is normal and thus has its normal resistance'. Based on this simplifying hypothesis, one assumes that each segment of the wire can only exist in one of the two distinct states: the superconducting, i.e. zero resistance state that occurs between phase slip events, and the normal state that is realized during each phase slip event in the considered segment. The resistance of the segment in this case equals its normal state resistance. To justify equation (1) we assume that the phase fluctuation attempt frequency Ω_0 and the relaxation time of the order parameter τ are defined by the same energy scale and hence related to each other as $\Omega_0 \approx 1/\tau$. The number of phase slips occurring per second, in accordance with the Arrhenius law, is $\Omega_{PS} = \Omega_0 \exp(-\Delta F/k_B T)$. The time fraction f during which each segment of the wire remains in the normal state is the product of the duration τ and the number of times the order parameter reaches zero per second, which is Ω_{PS}. Hence we get $f = \tau\Omega_0 \exp(-\Delta F/k_B T) \approx \exp(-\Delta F/k_B T)$. In this approximate model, during each unit of time, the wire stays normal during time f and remains superconducting

during time $1-f$. The fluctuations are very rapid, so only average values of the resistance can be detected. We define a set of independent equivalent segments in the wire, each having the length $\xi(T)$ and the normal state resistance $R_{1N} = R_N\xi(T)/L$, where L is the total length of the wire. The time average resistance of each segment is $\bar{R}_1 \approx R_{1N}f + R_0(1-f)$, where $R_0 \equiv 0$ represents the resistance of each segment in the superconducting state (i.e. when there is no phase slip core on it). Finally, the total resistance of the wire can be written as a product of the average resistance of each independent segment $\bar{R}_1$ and the total number of such segments $L/\xi(T)$. Thus one obtains equation (1), as follows:

$$R(T) = [L/\xi(T)]\bar{R}_1 = [L/\xi(T)][R_{1N}f + R_0(1-f)] = [L/\xi(T)][R_{1N}f] = R_N \exp(-\Delta F/k_BT).$$

7. LAMH theory in the limit of low bias currents

The normal resistance of the wire is not explicitly included in the LAMH theory, as it is the case in the Little's fit. The effective resistance is calculated by considering the time evolution of the superconducting phase $\varphi(x,t)$. The phase difference between the ends of the wire is $\Delta\varphi(t) = \varphi(L,t) - \varphi(0,t)$, where the coordinates of the wire ends are $x = 0$ and $x = L$. The supercurrent is proportional to the phase difference as $I_S = (e/m)|\psi|^2(\hbar\partial\varphi/\partial x - 2eA_x/c)$, with the phase gradient being $\partial\varphi/\partial x = \Delta\varphi/L$ if the supercurrent density is constant along the wire. Here and below, the charge of one electron is $e = -|e|$, the Planck's constant is $\hbar$ and the mass of an electron is m. Since the effect of magnetic field is not considered here, zero vector potential is chosen: $A_x = A_y = A_z = 0$.

If the charge transport is stationary, a dynamic equilibrium is established. For a constant bias voltage $V = \text{const}$, the supercurrent is also constant $I_S = \text{const}$ on average. Therefore the phase difference should, on average, satisfy $\mathrm{d}(\Delta\varphi)/\mathrm{d}t = 0$. Two processes contributing to the change of the phase difference $\Delta\varphi$: first, it is the voltage-driven phase rotation occurring at the ends of the wire where the voltage is applied. Second, it is the phase difference relaxation or unwinding occurring due to phase slip events. Hence, the phase difference evolves as $\mathrm{d}(\Delta\varphi)/\mathrm{d}t = 2eV/\hbar + \omega_L$, where ω_L is the net phase slippage rate. Thus, for a stationary charge transport we get the condition $\omega_L = -2eV/\hbar$. In order to calculate the resistance $R = V/I_S$ one needs to calculate the stationary value of the supercurrent I_S at which the condition

$$\omega_L \equiv \Omega_+ - \Omega_- = -2eV/\hbar \tag{2}$$

is satisfied. So the problem is reduced to finding the rate of phase slips as a function of the supercurrent and the temperature $\omega_L \equiv \omega_L(I_S T)$. The net rate of phase slippage is defined as $\omega_L = \Omega_+ - \Omega_-$, where Ω_+ is the rate corresponding to phase slips and Ω_- is the rate corresponding to anti-phase slips. Two different rates are introduced because, as the order parameter goes to zero, the phase difference can change by 2π or by -2π. The 2π phase change events will be called 'phase slips' since they reduce the supercurrent (if $I_S > 0$ to start with). The -2π phase change events will be called 'anti-phase slips'[3].

Consider an example: suppose the bias voltage is zero $V = 0$. In this case, due to equation (2), one needs to satisfy $\Omega_+ = \Omega_-$. The asymmetry between the phase slips and anti-phase slips depends on the supercurrent. The rates are equal if and only if the supercurrent is zero. Thus one concludes that $I_S = 0$ for $V = 0$. Hence a thin, nominally superconducting wire cannot support a current unless a nonzero voltage is applied.

First we discuss the energy barrier for phase slips in zero approximation, when the supercurrent is zero. For this it is necessary to find the difference of the wire's free energy in the equilibrium state, with a constant order parameter ($|\psi| = \psi_0$ const) and the 'phase slip state' that has a zero order parameter at some point $x = x_0$. Such solution has the form $|\psi| = \psi_0 \tanh[(x-x_0)/2\xi(t)]$ [81], with the phase difference between the ends of the wire $\Delta\varphi = \pi$. The exact calculation [37] shows that the energy barrier for a phase slip is $\Delta F(T) = V_{PS}(H_C^2/8\pi)$ where H_C is the temperature-dependent thermodynamic critical field, $V_{PS} \approx 3.77\xi A$ is the effective volume of the phase slip, A is the cross section area of the wire, and $\xi = \xi(T) = \xi(0)/\sqrt{1-T/T_C}$ is the temperature-dependent coherence length. At $I_S = 0$, the phase slip (PS) and the anti-phase slip (APS) rates are the same: $\Omega_+ = \Omega_- = \Omega\exp(-\Delta F(T)/k_BT)$, where $\Omega \approx (8k_B(T_C - T)/\pi\hbar)(L/\xi(T))\sqrt{\Delta F(T)/k_BT}$ is the attempt frequency [38, 39]. At $I_S > 0$ the barrier for phase slips becomes lower than the barrier for anti-phase slips (see equation (3) in [108], leading to a phase flow with the net rate $\omega_L = \Omega_+ - \Omega_- = \Omega[\exp(-(\Delta F - \delta F)/k_BT) - \exp(-(\Delta F + \delta F)/k_BT)]$. We use the usual notation $h = 2\pi\hbar$ and $R_Q = h/4e^2$. The barrier correction term $\delta F = \pi\hbar I_S/2e = eI_SR_Q$ equals one half of the difference between the barrier heights experienced by phase slips and anti-phase slips. The derivation of this correction, under the assumption that the supercurrent is constant is as follows:

$$\delta F = \int I_S V\,\mathrm{d}t = \int I_S[(2e)^{-1}\hbar\,\mathrm{d}\varphi/\mathrm{d}t]\,\mathrm{d}t = \int_0^\pi I_S(2e)^{-1}\hbar\,\mathrm{d}\varphi = \pi\hbar I_S/2e.$$

In other words, δF is the work done by the supercurrent over the system, as the phase difference between the ends of the wire increases by π, which corresponds to an evolution of the system from a state with a uniform order parameter to a 'phase slip state' that has zero order parameter at some point.

[3] As a phase slip occurs, the phase difference can change either as $\Delta\varphi \to \Delta\varphi + 2\pi$ (phase slip) or as $\Delta\varphi \to \Delta\varphi - 2\pi$ (anti-phase slip). In the general case the phase change can be written as $\Delta\varphi \to \Delta\varphi + 2\pi n$. The events characterized by an integer n and the condition $|n| > 1$ are higher order, less probable events, which are neglected. The phase jumps with n not an integer number are also neglected, due to the fact that they would require a rapid, as rapid as the phase slip event itself, change of the phase of the leads, which is not possible since leads are assumed macroscopic and the applied voltage is small. To further clarify this discussion we note that the phase difference between the leads is fully defined by the number of revolutions the wire's complex order parameter makes around the x-axis in the Little diagram (figure 5). This number of revolutions, which is, in fact, the phase difference $\Delta\varphi$, is a continuous variable and does not have to be an integer. But, topologically, a phase slip can only change the number of revolutions by an integer.

(As always, it is assumed that $I_S \ll I_C$.) If $I_S > 0$, the work performed by the current is positive for phase slips, and thus the barrier is reduced for them. The work is negative for anti-phase slips, and so the barrier for anti-phase slips is increased by the same amount. Using equation (2) we get:

$$-eV = \hbar\Omega \exp(-\Delta F/k_B T)\sinh(\delta F/k_B T) \approx \delta F(\hbar\Omega/k_B T)\exp(-\Delta F/k_B T). \quad (3)$$

Finally it is possible to write the corresponding resistance (LAMH resistance) $R_{LAMH}(T) = V/I_S$, as:

$$R_{LAMH}(T) = R_Q(\hbar\Omega/k_B T)\exp(-\Delta F(T)/k_B T) = Dt^{-3/2}(1-t)^{9/4}\exp[-c(1-t)^{3/2}/t] \quad (4)$$

with the normalized temperature defined as $t = T/T_C$. Normal quasiparticles, present in the wire at $T \sim T_C$, provide a parallel conduction channel. Thus the net resistance can be approximated as [39]

$$R^{-1} = R_{LAMH}^{-1} + R_N^{-1}. \quad (5)$$

Here R_N is the normal resistance of the wire. The LAMH model predicts the constants D and c as follows [27, 66]:

$$c \equiv \frac{\Delta F(0)}{kT_C} = \frac{1.76\sqrt{2}}{3}\frac{R_Q}{R_N}\frac{L}{\xi(0)} \quad (6)$$

and

$$D = (8/\pi)(L/\xi(0))R_Q\sqrt{c}. \quad (7)$$

8. Comparison with experiments

It the above discussion we outlined two possible theoretical models generating TAPS-based $R(T)$ curves, namely the Little's fit, which explicitly involves the normal resistance of the wire, and the LAMH model, which is based purely on superconducting phase behavior. In this section we present a comparative analysis of these two models, which was carried out on the example of narrow superconducting bridges [79]. The $R(T)$ curves are shown in figure 6. The direct low bias transport measurement is represented by open circles. The solid black circles represent the resistance determined by an indirect procedure, namely by extrapolation of high bias (nonlinear) $V(I)$ measurements to zero bias [79]. The Little's fit is shown as a solid red curve and the LAMH fit is shown as a dashed blue curve. Both curves exhibit a good agreement with the data points at low temperatures where the resistance drops rapidly. This agreement is observed over a range of eleven orders of magnitude of the resistance. Yet there is a significant difference between the two fits, as is apparent from the values of the critical temperature. In each of these two fits the critical temperature of the bridge is used as a free fitting parameter. The best Little fit is obtained with $T_{C,BRIDGE,Little} = 4.81$ K and the best LAMH fit is obtained with $T_{C,BRIDGE,LAMH} = 5.38$ K. By an independent direct measurement it was determined that the critical temperature of the film electrodes is $T_{C,FILM} = 4.91$ K in this sample. Thus the LAMH fit requires the critical temperature of the bridge to be chosen higher than that of the film electrodes connected to the bridge. At the same time, it is quite certain that in the actual sample the T_C of the bridge is

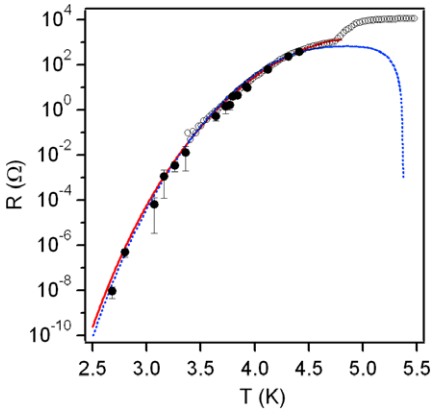

Figure 6. Resistance plotted versus temperature, for a narrow superconducting bridge sample B2 from [79]. Open circles represent direct low bias transport measurements of the sample resistance. Filled circles represent resistance determined indirectly, namely by extrapolating high bias segments of the nonlinear voltage–current $V(I)$ curves. The solid (red) and the dashed (blue) curves give the best fits generated by the Little (equation (1)) and LAMH (equation (4)) formulas correspondingly. The critical temperature of the bridge was used as a fitting parameter. The best fits were obtained with $T_{C,BRIDGE,Little} = 4.81$ K for the Little and $T_{C,BRIDGE,LAMH} = 5.38$ K for the LAMH fit. The critical temperature of the thin film electrodes is $T_{C,film} = 4.91$ K in this sample, which is, unrealistically, less than $T_{C,BRIDGE,LAMH}$.

either equal or lower than the T_C of the electrodes. The reason is that the bridge and the electrodes are made in the same sputtering run, consequently they have the same thickness[4]. It is also known that the T_C of MoGe films depends on the thickness of the film: the smaller the thickness is the lower the T_C is [1, 2]. It is also well established that if the film is shaped into a thin strip, the T_C drops even lower [83].

Hence it can be expected with certainty that the critical temperature of the bridge is equal or lower than the critical temperature of the film electrodes. The LAMH-generated critical temperature was in contradiction with this expectation. Thus it can be suggested that the Little fit might be a more accurate predictor of the critical temperature of a weak link, such as a nanobridge or, possibly, a nanowire. The deviation in the LAMH fit might be due to the fact that this fit generates zero resistance at the critical temperature (see the blue dashed curves in figure 6 going down as the temperature approaches the critical temperature $T_{C,BRIDGE,LAMH} = 5.38$ K). This unphysical artifact occurs due to the fact that the LAMH attempt frequency [38] approaches zero at the critical temperature of the bridge or of the wire. More accurate fits can probably be obtained by taking into account the phase diffusion phenomenon, which should prevent the attempt frequency from vanishing at $T \to T_C$ [84].

[4] The fabrication of the bridges in [79] was done in the same way as the fabrication of molecular-templated nanowires, outlined in the second section of this review. The only difference was that in the case of the nanobridges no molecule was used, but, instead, a SiN bridge served as a template for the superconducting bridge. Therefore such bridges are usually wider than nanowires produced by metal decoration of carbon nanotubes.

9. Quantum phase slips: Giordano's model

It is generally expected that any thermal activation over a barrier, such as the TAPS discussed above, would change to quantum tunneling at sufficiently low temperatures. Consequently, at low enough temperature phase slips should arise from quantum fluctuations of the order parameter. Observation of such quantum phase slips (QPS) was first reported by Giordano [25], in experiments with thin In and PbIn wires. The QPS phenomenon appeared as a crossover from the thermally activated behavior near T_C to a more weakly temperature-dependent resistance 'tail' at lower temperatures. Giordano suggested a model that describes the resistance tails in terms of macroscopic quantum tunneling (MQT) of quantum phase slips through the same free energy barrier as the one experienced by TAPS. However, interpreting these QPS results has been complicated by the reports in which thin wires were measured but such resistive tails were either not observed [5, 54, 53] or were weak and warranted a different interpretation [42]. Yet, the number of experimental reports in which some sort of resistance tail was observed and was discussed in terms of QPS is larger [25, 27, 55, 56, 58]. We present some of these results below. First, we review the Giordano model [25] for MQT of QPS, as outlined in [27].

It can be argued that the probability of QPS at very low temperatures should be proportional to $\exp(-\Delta F(0)/\hbar\omega_S)$, where $\hbar$ is the Planck's constant and ω_S is some characteristic frequency of quantum fluctuations of the superconducting order parameter [27]. The expression for the resistance in the case of QPS is similar to the pure TAPS case, but an extra term is added that represents the QPS contribution, namely the Giordano term R_G, assumed connected in series with the LAMH resistance, since the classical and quantum fluctuations contribute additively to the total rate of phase slip events. For this reason the total resistance is written as:

$$R^{-1} = (R_G + R_{LAMH})^{-1} + R_N^{-1}. \tag{8}$$

A heuristic argument leads to a conclusion that the resistance originating from the QPS follows a form similar to the LAMH expression (equation (4)), except that the appropriate quantum fluctuation energy scale is $k_B T_Q = \hbar/\tau_{GL} = (8/\pi)k_B(T - T_C)$, instead of the usual thermal energy $k_B T$. Thus the quantum Giordano resistance is [27]:

$$R_G = B\,R_Q(\hbar\Omega_G/k_B T_Q)\exp[-a\Delta F/k_B T_Q] \tag{9}$$

with two extra adjustable parameters B and a which are supposed to be of order unity. These parameters take into account the approximate nature of the suggested expression [27]. Following the same idea of replacing the thermal energy $k_B T$ by the 'quantum energy' $k_B T_Q$ in the thermal attempt frequency, the following approximate form for the quantum attempt frequency can be written [25, 27]:

$$\Omega_G = (k_B T_Q/\hbar)(L/\xi(T))\sqrt{\Delta F(T)/k_B T_Q}. \tag{10}$$

Since QPS are expected to occur even at zero temperature, one concludes that such QPS model presumes that any superconducting wire has a finite resistance even at zero temperature. So, strictly speaking, superconductor–insulator transition does not occur, because the truly superconducting phase does not exist within this model.

From equations (4) and (9) it follows that the ratio of the quantum Giordano and classical LAMH terms can be written as $\rho_{QC} = R_G/R_{LAMH} = B(\pi t/8(1-t))^{3/2}\exp[c\sqrt{1-t}((1-t)/t - a\pi/8)]$. Here the parameter c is defined in equation (6) and a and B are unknown parameters of order unity. The quantum contribution exceeds the classical one if the temperature is low enough so that $\rho_{QC} > 1$. This condition is satisfied if the temperature is, approximately, $T < 0.7T_C$. The ratio ρ_{QC} of the quantum and thermal contributions is plotted in figure 10 (inset). The inset shows computed plots of $\rho_{QC} \equiv R_{MQT}/R_{LAMH}$ versus $t \equiv T/T_C$ for typical values $c = 8$, 16, 24, 32, 40, with the assumption that $a = 1$ and $B = 1$. The temperature $T^* = 0.718T_C$ appears as a universal temperature below which the Giordano model predicts a higher QPS rates compared to the TAPS rate. The temperature T^* is almost independent on the choice of the factors a and B. The knowledge of the T^* is important for the analysis of experimental $R(T)$ curves. As the temperature is reduced, the resistance drops and quickly goes below the 'noise floor', which, in many direct transport measurements on nanowires, is in the range of 1–10 Ω. Thus one concludes that the quantum Giordano contribution can only be observed in experiments, in which the wire is thin enough and the set-up is sensitive enough so that the resistance is still measurable (i.e. above the noise level) at $T \approx 0.7T_C$ and somewhat lower than this.

It can be noted that the situation is different in very thin wires. The plots of figure 10 (inset) show that for wire with $c < 8$ the quantum contribution to the phase slip rates is larger than the classical contribution at *all* temperatures. One can estimate the corresponding critical diameter d_C at which such quantum regime begins. For this, we use equation (6) to get $L/R_N = 3c\xi(0)/1.76\sqrt{2}R_Q$, where $L/R_N = A_C/\rho = \pi d_C^2/4\rho$. The resistivity for $Mo_{79}Ge_{21}$ is $\rho \approx 200\ \mu\Omega$ cm $= 2$ kΩ nm. Thus one gets $d_C = \sqrt{12\rho c\xi(0)/1.76\sqrt{2}\pi R_Q} \approx 6.2$ nm with the assumption that the length of the wire is $L = 100$ nm, the coherence length is $\xi(0) = 10$ nm and the parameter $c = 8$ (as the threshold for completely quantum behavior). It is interesting to note that such estimated critical diameter is indeed quite close to the diameter at which an SIT is observed, at least for wires of length $L \approx 100$ nm. The relevance of this observation to the explanation of the SIT in nanowires is unknown.

10. Transport measurements and comparison with the LAMH theory and the Giordano model

A practically useful classification of samples based on their $R(T)$ curves is illustrated by figure 7. The classification is as follows: 'S', superconducting or 'truly superconducting' behavior, is defined as such that $dR/dT > 0$ and $d^2(\ln R)/dT^2 < 0$; 'N1', normal and strongly conducting, behavior is defined by the conditions $dR/dT > 0$ and $d^2(\ln R)/dT^2 > 0$ (the N1 type of the $R(T)$ curve is also called a 'resistive tail'); 'N2', normal and weakly conducting, is defined by the conditions $dR/dT < 0$ and $d^2(\ln R)/dT^2 <$

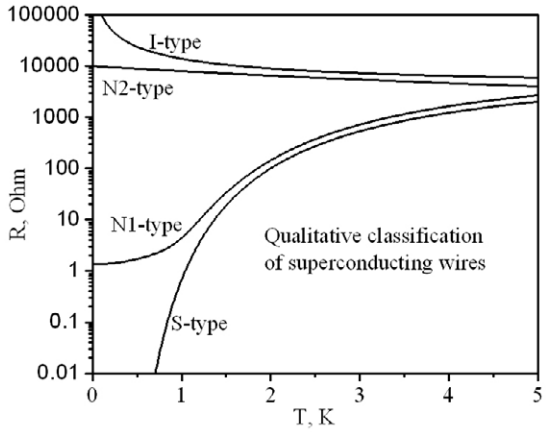

Figure 7. Empirical qualitative classification of nanowires made of superconducting metals. These include truly superconducting wires (S), having a resistance that quickly decreases with cooling, resistive or 'normal' wires (N1 and N2) and insulating wires (I), having their resistance growing with cooling, without apparent saturation. The difference between the two types of resistive wires, namely N1 (strongly conducting) and N2 (weakly conducting), is that N1 is characterized by a resistance that drops with cooling and saturates at some temperature, while N2 type exhibits a resistance that increases slightly with cooling and also approaches a finite limit as the temperature approaches zero. The N1 type of the $R(T)$ curve is also called a 'resistive tail'.

0; and, finally, 'I', the insulating one is defined by the conditions $\mathrm{d}R/\mathrm{d}T < 0$ and $\mathrm{d}^2(\ln R)/\mathrm{d}T^2 > 0$. Thus, for example, both superconducting (S) and normal strongly conducting (N1) samples are characterized by resistance decreasing with cooling. The difference between them, within this classification, is that S samples exhibit a negative curvature on the log-linear $R(T)$ plots while N1 samples exhibit a positive curvature. Naturally, we also assume that if $R(T) \to R(0) > 0$ in the limit $T \to 0$, then the sample is either N1 type (if $R(0) < R_N$) or N2 type (if $R(0) \geqslant R_N$). If, on the other hand, the resistance drops very rapidly with cooling, say as $R(T) \sim \exp(-1/T)$, then it is expected that $R(T) \to 0$ in the limit $T \to 0$. Such a sample is classified as S type, in agreement with the definitions given above. Evidently, these classifications are only approximate since the measurements are usually done down to $T \sim 10$ mK in the best cases and it is not known what happens to the sample conductance below this limit. Also, the 'noise floor' for the resistance is typically above 1 Ω, for usual values of the bias current chosen in the range 1–10 nA. The behavior of the resistance below this level is usually not known. One qualitative physical interpretation of the classification introduced above can be this: the S regime corresponds to the TAPS process, with a negligible QPS rate; the N1 regime corresponds to the TAPS process with a noticeable contribution of the QPS; the N2 regime corresponds to a strong and dominant QPS process, and the I regime corresponds to 'proliferating' QPS, which completely eliminate the ability of the wire to carry a supercurrent and possibly destroy the condensate completely, due to the collective effect of the normal cores of the QPS [54].

Experimentally, samples of the type N1 and N2 are not observed among homogeneous and *short* samples [5, 53, 59, 80].

Table 1. Parameters of short wires, studied in [5]. The wire's length, L, and the width, w, are measured under the SEM. Note that the measured width w is expected to exceed considerably the actual width of the metallic core of the nanowire. This overestimation of the width is due to the presence of the surface oxidized layer. The parameter R_N is the normal state resistance, defined as is illustrated in figure 3, t is the nominal thickness of the sputtered film, which is assumed to be equal to the thickness of resulting wires. The diameter d_{CALC} is calculated from R_N and L as $d_{CALC} = \sqrt{4L\rho/\pi R_N}$. The resistivity used in this calculation was chosen $\rho = 2.35$ kΩ nm. The exact value of the resistivity is not well-known, but various estimates give values scattered between 1.8 and 2.5 kΩ nm. The parameter c is calculated as $c \equiv \Delta F(0)/kT_C = (1.76\sqrt{2}/3)[L/\xi(0)](R_Q/R_N)$ [82].

Sample	L (nm)	w (nm)	D_{CALC} (nm)	t (nm)	R_N (kΩ)
A	99 ± 10	21 ± 3	11.1	8.5	2.39
B	127 ± 10	19 ± 3	11	8.5	3.14
C	93 ± 10	17 ± 2	8.8	8.5	3.59
D	109 ± 12	13 ± 3	8.3	7.0	4.73
E	116 ± 12	12 ± 4	7.9	7.0	5.61
F	125 ± 7	14 ± 4	7.8	7.0	6.09
G	105 ± 8	11 ± 2	6.2	5.5	8.22
H	121 ± 14	9 ± 2	6.5	5.5	8.67
I	140 ± 9	11 ± 2	6.6	5.5	9.67
J	86 ± 15	14 ± 3	3.1	7.5	26.17

In this review, we use the term 'short' referring to the samples shorter than about 200 nm. This is an empirical length threshold, such that longer wires frequently show the N1 and N2 types of behavior, while the short wires usually either belong to the S type or the I type. Samples of types N1 and N2 were reported in, for example, [27, 55, 85, 86]. Some of these examples will be discussed at the end of this section and compared to the Giordano model. Also, some of the inhomogeneous samples exhibit N1 behavior. In general, inhomogeneous wires show a complicated behavior, which goes beyond the simple classification of figure 7. They are excluded from our discussion in this review. Inhomogeneous wires are easily identified by multiple steps in their $R(T)$ curves as well as by multiple critical current peaks in their $\mathrm{d}V/\mathrm{d}I$ versus I curves. For more details on the fabrication and the properties of inhomogeneous wires see the corresponding sections in [5]. It is notable that in experiments on thin superconducting films a similar trend is found, i.e. granular films shows the N1 behavior while homogeneous films show either the S or the I type [6].

A representative study of *short* wires, made of amorphous $Mo_{79}Ge_{21}$, was reported by Bollinger *et al* [5, 66]. The parameters of these wires are given in table 1. These were unprotected MoGe wires sputter deposited over fluorinated single-wall carbon nanotubes.

Resistance versus temperature plots for the samples listed in the table 1, are shown in figure 8(a). All these samples have $L < 200$ nm, i.e. these are short samples. It comes into view that some samples exhibit a rapid decrease representing an Arrhenius type activation dependence of the resistance on temperature, while others remain strongly resistive down to the lowest temperatures and exhibit some increase of the resistance as T decreases. The samples A, B, C, ZZ, and YY are clearly of the S type: their resistance drops rapidly and the curves exhibit a negative curvature. The $R(T)$ curves of samples

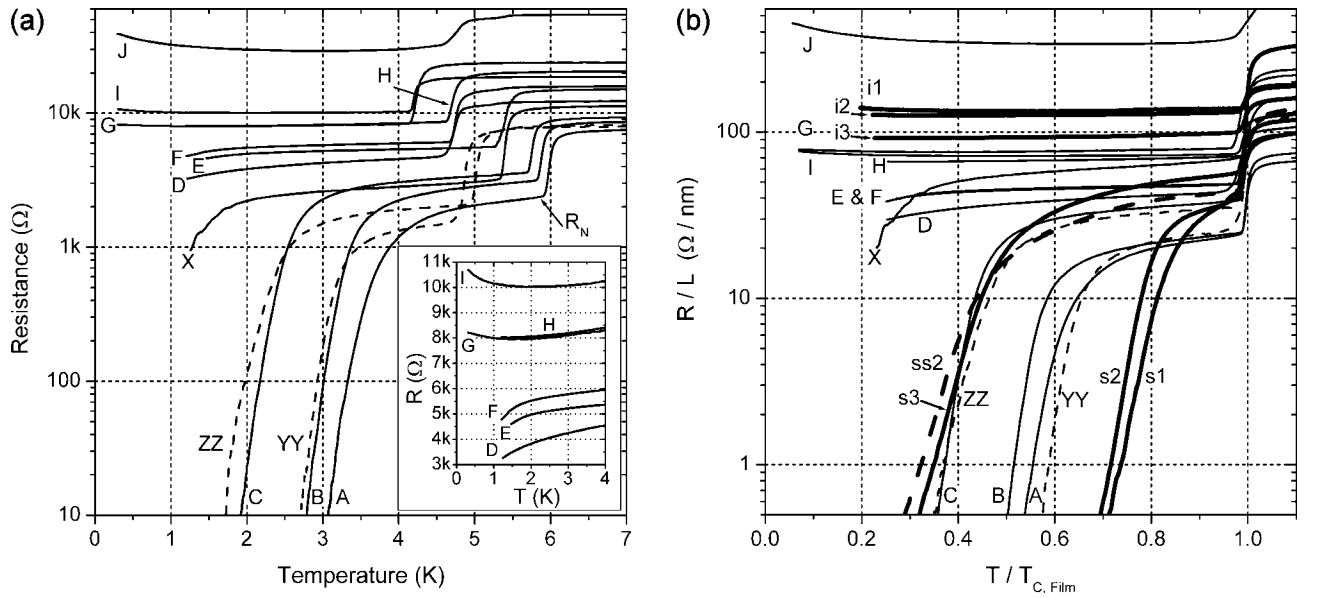

Figure 8. Resistance versus temperature of MoGe nanowires listed in table 1 [5]. Each curve represents a different sample. The difference between the samples is the amount of MoGe sputtered, and the width and the length of the nanotube (or possibly a nanotube rope) that supports the wire. (a) Log-linear plots of zero-bias resistance versus temperature. The dashed curves represent double-wire samples. (Inset) The same $R(T)$ data magnified near R_Q, showing that the behavior changes from S type to I type at $R_N \approx 6.5$ kΩ. (b) Resistance divided by the length is plotted versus the temperature normalized by the critical temperature of the film. This combined plot includes all samples listed in table 1 and also samples from [26] (thicker lines). The transition from S type to I type behavior is observed at $R_N/L \approx 60\ \Omega\ \mathrm{nm}^{-1}$. One shorter sample, X, behaves as a superconducting wire, although it has a high value $R_N/L \approx 70\ \Omega\ \mathrm{nm}^{-1}$.

F, E, D, and X suggest that they are also S type, since they satisfy the conditions $\mathrm{d}R/\mathrm{d}T > 0$ and $\mathrm{d}^2(\ln R)/\mathrm{d}T^2 < 0$. Unfortunately, these samples were measured only down to $T \approx 1.3$ K so it is not possible to conclude with certainty that their S type behavior would continue to lower temperatures. The samples G, H, I, and J clearly satisfy the conditions for the I type regime as they all satisfy the conditions $\mathrm{d}R/\mathrm{d}T < 0$ and $\mathrm{d}^2(\ln R)/\mathrm{d}T^2 > 0$. Thus, if the inconclusive samples (E, F, D, X) are either excluded or assumed to continue their S type behavior down to low temperatures, this entire set of samples (figure 8(a)) exhibits a dichotomy, with an S-to-I transition. This set of plots strongly suggests that a quantum superconductor–insulator transition (SIT) takes place, as the wires are made thinner and more resistive. The transition takes place at some critical value of the wire's normal state resistance, which equals, approximately, $R_Q = h/4e^2 \approx 6.5$ kΩ. (The conventional exact value of the von Klitzing constant is $R_K = h/e^2 = 25\,812.807\ \Omega$ [87]. For paired electrons, the exact value therefore is $R_Q = h/4e^2 = 6453.224\,25\ \Omega$.)

In order to verify whether the SIT critical point is associated with some critical diameter or a critical value of the wire cross section area A, we re-plot the data in a different format. In figure 8(b) the ratio $R/L = \rho/A$ is plotted versus temperature, normalized by the critical temperature of the film electrodes, following [27]. The samples from [26] are also included for comparison, as thick solid curves. These older results show a general agreement with the samples taken from [5], regardless the fact that different types of nanotubes were used in the fabrication process: ordinary tubes—in [26] and insulating fluorinated tubes—in [5]). The entire collection of samples satisfies approximately the following conditions: samples with $R_N/L < 60\ \Omega\ \mathrm{nm}^{-1}$ appear superconducting and those with high $R_N/L > 60\ \Omega\ \mathrm{nm}^{-1}$ turn out insulating. Thus, some type of dichotomy is apparent in this presentation also. Yet, due to the fact that all analyzed wires were of a similar length, it is not possible to establish definitely whether the critical point of the observed SIT is defined by a critical resistance or by a critical cross section area. The sample X, which was a shorter sample and had $R_N/L \approx 70\ \Omega\ \mathrm{nm}^{-1}$, still shows an S type behavior. This sample tilts the balance in favor of the assumption that the total normal resistance is the proper control parameter. This trend was later confirmed by a study of wires of different length [53].

One way to analyze such data (figure 8(b)) quantitatively was proposed by Golubev and Zaikin [57]. Their model predicts a rapid crossover rather than an SIT. In the model the crossover from an approximately superconducting to approximately normal behavior takes place at $R_N/L \sim 60\ \Omega\ \mathrm{nm}^{-1}$, which corresponds to $A_C = \rho(L/R)_C \sim 33\ \mathrm{nm}^2$, obtained assuming that the resistivity is $\rho = 2000\ \Omega$ nm. Thus the critical diameter is $d_C = \sqrt{4A_C/\pi} \sim 6.5$ nm. This result is in an approximate agreement with the data (figure 8(b)). It is also in agreement with our above estimation, based on the Giordano model, of the critical diameter at which the QPS rate exceeds the TAPS rate at all temperatures (see the discussion above and figure 10, inset).

Strong evidence in favor of SIT was reported by Bollinger *et al* in [54]. The corresponding $R(T)$ curves are re-plotted in figure 9. The top figure (figure 9(a)) accumulates all samples which showed the insulating behavior, while the bottom graph (figure 9(b)) presents all other homogeneous wires, all of which

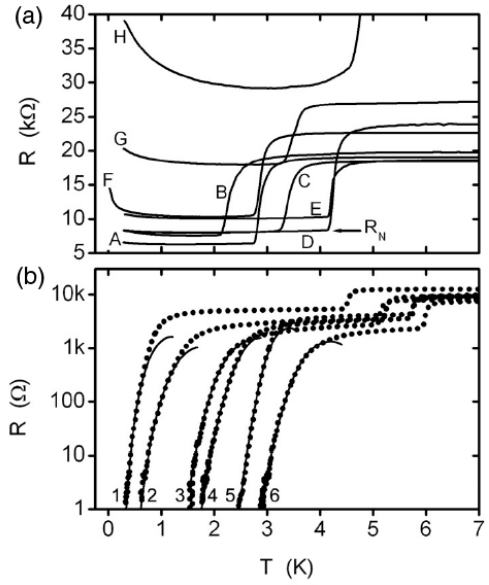

Figure 9. Sets of $R(T)$ curves for insulating and superconducting wires are shown in (a) and (b) correspondingly. The measurements were made by Bollinger *et al* [54]. The horizontal arrow in (a) illustrates how the normal resistance R_N is defined, using the example of sample D. For samples A–H, the corresponding normal resistances of the wires was $R_N = 6.43$, 7.54, 8.25, 8.35, 10.33, 10.50, 18.05, and 32.46 kΩ. The corresponding lengths of these wires were 46, 45, 140, 105, 140, 49, 120, and 86 nm. In (b), solid curves indicate fits to the LAMH model, which represent the resistance drop, occurring due to freezing out of TAPS. The fitting parameters, namely the coherence lengths, 70.0, 19.0, 11.5, 9.4, 5.6, and 6.7 nm, and the critical temperatures, 1.72, 2.28, 3.75, 3.86, 3.80, and 4.80 K were used to calculate the fitting curves for samples 1–6 correspondingly. The corresponding normal resistances and the lengths were 5.46, 3.62, 2.78, 3.59, 4.29, 2.39 kΩ and 177, 43, 63, 93, 187, 99 nm, respectively. Note that all superconducting samples are shorter than 200 nm and have their normal resistance below the quantum resistance constant, ∼6.5 kΩ. An alternative interpretation of the superconducting samples, based on the QPS phenomenon and involving slowing down of the QPS by the Caldeira–Leggett mechanism, was recently advanced in [45].

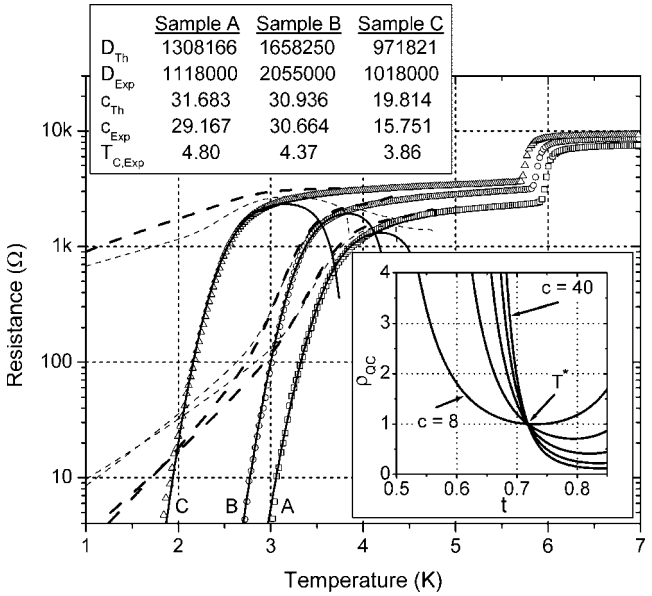

Figure 10. $R(T)$ data (open symbols) for samples A, B, and C compared to the LAMH theory of TAPS (continuous lines) [66]. The table shows the best LAMH fitting parameters c_{Exp}, D_{Exp}, and T_C and compares them to the computed parameters (c_{Th} and D_{Th}). The dashed lines show the predictions of the Giordano model (equation (8)), which includes quantum phase slips. Heavy dashed lines correspond to $a = 1.3$, $B = 7.2$. The thin dashed lines were computed with $a = 1$, $B = 1$. The coefficients a and B have been introduced in [27] in order to account for the absence of exact knowledge about the ratio of attempt frequencies and the barrier shapes, which influence the QPS and TAPS rates. Inset: computed plots of $\rho_{QC} \equiv R_{MQT}/R_{LAMH}$ versus $t \equiv T/T_C$ for $c = 8$, 16, 24, 32, 40 (assuming $a = 1$ and $B = 1$). The temperature $T^* = 0.718\ T_C$ is a universal temperature below which the Giordano model predicts a higher QPS rates compared to the rate of TAPS.

showed the S type behavior. The observed dichotomy is an indication of a quantum SIT. The transition takes place as the normal resistance of the nanowire reaches some critical value, which is close to R_Q. We note that all the wires shown in figure 8 have similar lengths, $L \sim 100$ nm. Again, this set of samples is not sufficient to establish, with certainty, whether the total normal resistance R_N of the wire is the control parameter for the SIT, or it is the cross section area A of the wire. A set of samples of widely varying lengths should be measured in order to establish whether a global characteristic, such as R_N, or a local characteristics, such as A, controls whether the wire belongs to S type or to I type.

An investigation of a set of samples with a wide variety of lengths was recently reported by Bollinger *et al* [53]. It was shown there that the critical resistance condition $R_{N,C} = \text{const} \approx R_Q$ provides a better description of the SIT phase boundary, compared to the critical cross section condition $A_C = \text{const}$, especially if only the short wires ($L < 200$ nm) are included in the analysis. Yet, the expression $R_{N,C} = \text{const} \approx R_Q$ was also not in perfect agreement with the data. Bollinger *et al* found experimentally (see figure 4 in [53]) that the exact phase boundary can be expressed as a length-dependent critical resistance. According to them, the SIT takes place at the critical normal resistance $R_{N,C} = 2R_Q/(1 + l_0/L)$, where the experimentally determined characteristic length constant was $l_0 \approx 107$ nm. Three limiting cases can be defined based on this formula: (i) very short wires ($l_0/L \gg 1$) become insulating as their cross section is reduced below the critical value $A_C = \rho l_0/2R_Q$. (ii) Very long wires ($l_0/L \ll 1$) become insulating at $R_{N,C} = 2R_Q/(1+l_0/L) \approx 2R_Q$. (iii) Intermediate wires ($l_0/L \approx 1$) become insulating as their normal resistance exceeds the critical value $R_{N,C} = 2R_Q/(1 + l_0/L) \approx R_Q$. Note that the second case ($l_0/L \ll 1$) allows a simple interpretation: long wires become insulating as soon as all single-electron quantum states become localized, i.e. when the resistance of the wire becomes half the von Klitzing constant, $R_{N,C} \approx 2R_Q = h/2e^2$. Very short wires may be controlled by a critical diameter, possibly due to expected presence of magnetic moments in their surface [53, 80]. Complete understanding of the phase boundary, however, is still lacking.

Now, following Bollinger [66], we compare the $R(T)$ curves of short MoGe samples with the LAMH model and the Giordano model. Figure 10 shows $R(T)$ plots for samples A,

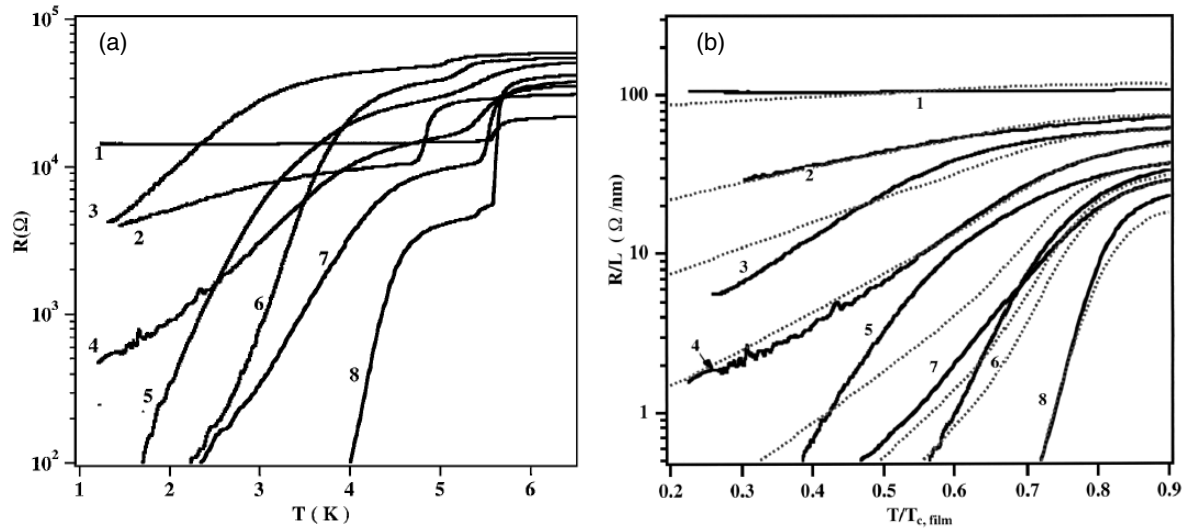

Figure 11. (a) Resistances versus temperature curves for a set of longer MoGe wires (up to 1000 nm long) [27]. The wire's normal state resistances and lengths are 1: 14.8 kΩ, 135 nm; 2: 10.7 kΩ, 135 nm; 3: 47 kΩ, 745 nm; 4: 17.3 kΩ, 310 nm; 5: 32 kΩ, 730 nm; 6: 40 kΩ, 1050 nm; 7: 10 kΩ, 310 nm; 8: 4.5 kΩ, 165 nm. (b) Resistance divided by the length plotted versus temperature, normalized by the critical temperature of the film electrodes is plotted. The solid lines are the data. The dotted lines are calculated using the Giordano model of quantum phase slips (see equations (8) and (9)). The two fitting parameters that produced the best agreement with the experiment curves are $a = 1.3$ and $B = 7.2$. They were used for the entire family of experimental curves.

B, and C (from figure 8(a)) together with the LAMH fits (solid lines) computed using equation (4). The fits show a nearly perfect agreement with the data, except very near T_C, where the LAMH theory is not applicable (due to the zeroing of its attempt frequency) [39]. The experimental fitting constants c_{Exp} and D_{Exp} are in good agreement with equations (6) and (7). Thus these wires act as homogeneous 1D superconductors, well described by the LAMH model, without inclusion of the QPS. This fact gives evidence that the wires are true superconductors (S type).

The dashed lines show the predictions of the Giordano model (equation (8)), which includes QPS. The thick dashed lines correspond to $a = 1.3$, $B = 7.2$, found experimentally for longer wires by Lau *et al* [27]. The light dashed lines correspond to generic values, $a = 1, B = 1$. In this example, the QPS inclusion leads to a strong overestimation of the wire resistance. This regime can be called 'truly superconducting' since the QPS rate is strongly suppressed and the results are explained in terms of TAPS. We speculate that the observed absence of the QPS contribution to the resistance might be due to the QPS suppression caused by some coupling to the environmental dissipative reservoir, i.e. due to the Caldeira–Leggett mechanism [47, 48]. The dissipative bath may be provided by plasma waves in the leads [44] as well as quasiparticles in the wire, which may be produced by a collective action of multiple QPS.

Now we turn our attention to longer wires. A study of wires up to ∼1000 nm in length was reported in [27]. The behavior of longer wires was qualitatively different from the short wires, discussed above. The main difference was that the sharp dichotomy indicating the SIT was not observed in the set of longer wires. On the contrary, a smooth crossover from strongly superconducting to weakly superconducting wires and then to normal-like wires was observed (figure 11(a)). Most of the wires in the group shown in figure 11 exhibit resistive tails, which were not found in the group of, on average, shorter wires, such as those shown in figure 9(b). The resistive tails are a sign of QPS. Indeed, it was possible to fit, approximately, the entire series of $R(T)$ curves (figure 11(b)) using the Giordano model (equation (8)), with only two fitting parameters. The coefficients a and B are unknown and were used as free fitting parameters.

The reason for the apparently different behavior in short and longer wires is not well understood. Nevertheless, it should be pointed out that the normal resistance of all wires in the set of figure 11 was above R_Q, while the normal resistance of all truly superconducting (S type) wires (figures 8–10) is below R_Q. All observations can be summarized by saying that wires with $R_N < R_Q$ tend to be of S type, while the wires with $R_N > R_Q$ tend to be either I type, if they are very thin, or N1 type or N2 type, if the diameter is relatively larger. Since most of the wires presented in figure 11 satisfy $R_N > R_Q$ (except sample #8), the QPS is not fully suppressed in any of these wires (except #8, in which the QPS 'tail' is not present). Yet, the QPS rate can be different (and may not always be sufficient to produce I type regime), as it is dependent on the cross section of the wire [57], which is inversely proportional to the ratio R/L. So, on figure 11(b) one finds that wires with a low value of R_N/L (i.e. thicker wires) show a moderate level of QPS (i.e. rather low resistance), while wires with larger values of R_N/L (which are thinner) show a higher resistance and, some of them, even the I type behavior. Thus, the insulating behavior requires two conditions: first, $R_N > R_Q$ in order for QPS to be present at all, and, second, $R_N/L > 60$–$70\ \Omega\ \mathrm{nm}^{-1}$, in order for the QPS to be frequent enough to accomplish a complete suppression of the condensate. For short wires, the second condition is immediately satisfied as soon as the first is reached (by reducing the diameter). For longer wires, on

the other hand, the first condition may be satisfied, while the second is not, resulting in resistive tails (e.g. samples 6 and 7 in figure 11(b)).

11. Coulomb blockade in insulating wires

Short nanowires, which act as insulators (I type) have been analyzed in terms of the Coulomb blockade by Bollinger *et al* [54]. It was concluded that the apparent SIT transition occurs between a truly superconducting phase and an insulating phase, in which the condensate is eliminated in the wire, possibly due to a collective effect of a large number of QPS, each of which possesses a normal core. The insulator-like behavior is then induced by weak Coulomb blockade. Below we review these results.

Figure 9(a) shows $R(T)$ curves for a set of insulating wires. To understand the observed $\mathrm{d}R/\mathrm{d}T < 0$ for all these samples, we compare the results to the theories of weak Coulomb blockade (CB) in diffusive normal wires. Nazarov showed [88] that the CB can survive in a setting in which two plates of a capacitor C are connected by a coherent, homogeneous normal wire, instead of the usual tunnel junction. The term 'coherent' implies that the wire is short enough, so that electrons can propagate through the entire wire without experiencing inelastic collisions. Thus, quantum phase coherence is maintained for electrons diffusing through the wire from one electrode to the other (or, in this model, from one plate of the capacitor C to the other). In this case, the entire nanowire plays the role of a tunnel barrier, in which the wavefunction amplitude decays exponentially, with a characteristic decay length given by the localization length. Thus, the nanowire is similar to a tunnel barrier, in which the wavefunction amplitude decays exponentially also, but on a much shorter length scale. For this reason, electrons can 'tunnel' through a diffusive nanowire over a much longer length scale compared to ∼1 nm scale in ordinary tunnel junctions. In other words, the entire nanowire acts as a coherent scatterer [89]. It should be emphasized that within this approach it is not assumed that the nanowire has some sort of a break, or a grain boundary, or any sort of weak links that would play a role of a tunnel barrier. On the contrary, the entire disordered homogeneous wire acts as an effective tunnel barrier, due to Anderson localization in disordered quasi-one-dimension (quasi-1D) system.

Since the 1991 work of Punyakov and Zaikin [90], it became clear that the Coulomb blockade survives even if the barrier resistance is much lower than $R_K = h/e^2$. And this is true for nanowires also: the CB does exist even in systems with wires having $R_N \ll R_K$ [88, 89, 91, 92]. Of course, the higher the barrier (wire) conductance, the weaker the Coulomb blockade effect. Golubev and Zaikin (GZ) [89] derived useful formulas for current–voltage $I(V)$ curves, enabling a direct comparison with the experiment. The result is generally applicable to a coherent scatterer of any type, including short thin wires and tunnel junctions. Again, the model considered includes a capacitor C shunted with coherent scatterer, i.e. a short enough mesoscopic diffusive wire or a tunnel junction. The main prediction of the theory is the current in this connecting element, for the case when the voltage on this capacitor is set. According to the GZ theory, at high temperatures (i.e. such that $k_BT \gg E_C$, where $E_C = e^2/2C$), the zero-bias conductance, $G(T) = 1/R(T) = I/V$ is:

$$G(T)/G_0 = 1 - \beta[(E_C/3k_BT) - (3g_0\varsigma(3)/2\pi^4 + 1/15)(E_C/3k_BT)^2]. \quad (11)$$

Here the parameter characterizing the distribution of conducting modes of the wire is defined as $\beta = \sum_n T_n(1-T_n)/\sum_n T_n$. For a tunnel junction, all the transmissions of the conducting modes are low, i.e. $T_n \ll 1$, so that $\beta = 1$. For a diffusive coherent wire the result is $\beta = 1/3$ [89]. Other parameters are $\zeta(3) = 1.202$, $g_0 \equiv G_0R_K$, and G_0 is the conductance of the scatterer in the absence of the CB, i.e. at high temperatures or high bias.

It is interesting to note that formally the same expression as equation (11) was derived by Joyez and Esteve [93] for a solitary tunnel junction, connected to macroscopic measurement leads. In this case the current suppression due to electron–electron repulsion is called the dynamic Coulomb blockade. Equation (9) in [93] is formally the same as our equation (11) (see above). The only difference is that in their case $\beta = 1$, since a tunnel junction was considered, and the value of the normalized high temperature limit conductance g_0 is replaced by the normalized 'environmental' conductance: $g_{J-E} \equiv R_K/R_{env}$, with R_{env} being the impedance of the environment.

Since the ratio E_C/k_BT is a small parameter, the $1/T$ and $1/T^2$ terms of equation (11) can be eliminated by introducing the Pekola type conductance function $\gamma(T) \equiv G_0(G_0 - G(T))^{-1}$. Then equation (11) assumes a particularly simple, linear form:

$$\gamma(T) \equiv \gamma(T) \equiv G_0(G_0 - G(T))^{-1} = A + BT \quad (12)$$

where constants following from the GZ theory are

$$A = (9/\beta)(3g\varsigma(3)/2\pi^4 + 1/15) \quad \text{and} \quad B = 3k_B/\beta E_C. \quad (13)$$

Historically the linearity of the $\gamma(T)$ function was discovered by Pekola and collaborators in their analysis of weak Coulomb blockade on systems involving two tunnel junctions connected in series and forming a single-electron tunneling (SET) transistor [94]. They found that at high temperatures the gate-induced Coulomb oscillation is smeared by thermal fluctuations, but a correction to the conductance of the entire device remains significant even at high temperatures, $k_BT/E_C \gg 1$. Their calculation is based on the Averin and Likharev Orthodox theory of single-electron tunneling [95]. An approximate solution of the Orthodox theory dynamic equations in the limit of high temperatures is $\gamma(T) \equiv A + BT$, with $A = 0$ and $B = 3k_B/E_C$. In this example the charging energy is defined as $E_C = e^2/2C_\Sigma$ and $C_\Sigma = 2C + C_g$ is the total capacitance of the Coulomb island of the SET device, with C_g being the capacitance of the Coulomb island to the ground. The capacitance of each junction is C. The conductance function (Pekola function) $\gamma(T) \equiv G_0(G_0 - G(T))^{-1}$ is defined here with $G_0 = 1/2R_0$, where R_0 is the resistance of

each junction in the limit of very high temperatures when the CB effect is completely suppressed. Note that the parameter B agrees with the GZ more general expression (equation (13)), since for tunnel junctions $\beta = 1$. The only qualitative difference is that the GZ theory predicts an offset A (possibly because it takes into account higher order corrections), while the result of Pekola *et al* is that $A = 0$.

Unlike systems with two tunnel junctions connected in series (as is the case in SET transistors), a solitary tunnel junction, connected to measurement leads, can naively be expected to show no charging effects (no CB), unless a substantial impedance, intimately connected in series with it, is present. Such argument might follow from the fact that the macroscopic leads, between which the tunnel junction is created, would have a very large mutual capacitance, rendering the CB phenomenon unobservable. Indeed, a typical value of the mutual capacitance of signal leads in a cryostat can be roughly estimated ∼100 pF. The corresponding charging energy would be 10 μK, which is ∼1000 times lower than the lowest temperature at which an SET device can be measured with present-day refrigerators. If the phenomenon of single-electron tunneling is analyzed as a high frequency phenomenon, still, one comes to the same conclusion since the impedance of the leads is usually of the same order of magnitude as the vacuum impedance $\sqrt{\mu_0/\varepsilon_0} \approx 377\ \Omega$, which is much lower than the resistance threshold $h/e^2 \approx 26\ \mathrm{k}\Omega$ above which the CB phenomenon becomes prominent. Thus it might seem impossible to observe any trace of the Coulomb blockade on a system involving just one tunnel junction, which couples two macroscopic leads with negligible resistance. Yet this is not the case. Experimentally, a significant zero-bias anomaly, in the form of a conductance deep, exists in single junctions [96–99]. A plausible explanation to these results was advanced by Kauppinen and Pekola, in terms of weak Coulomb blockade combined with a phenomenological Coulomb 'horizon' model [100]. They also carried out measurements on solitary tunnel junctions in order to corroborate their model. This suggested horizon model is a simplified version of the rigorous environment SET theory [101, 102, 93], and therefore it is intuitively more transparent. Qualitatively speaking, the Coulomb horizon defines the segment size of the electrodes, connected to the tunnel junction, which is involved in the single-electron tunneling events. This horizon allows one to define a finite effective capacitance, and thus a non-zero charging energy, even in the case when the leads are infinitely long. This horizon effect has also been discussed by Delsing *et al* [103] and by Wahlgren *et al* [99]. This same 'horizon' model can be applied to single nanowires since, as was pointed out above, a short nanowire is analogous to a tunnel junction. Without going into details we just list the Kauppinen and Pekola result for a solitary tunnel junction. Similar to the case of two junctions, the conductance function here is, again, linear $\gamma(T) \equiv G_0/(G_0 - G(T)) = A + BT$, with the same value of the slope $B = 3k_B/E_C$ and a non-zero (due to the horizon effect) offset value $A = 3c_L c\hbar/e^2$, where c_L is the capacitance per unit length of the conductor strip attached to the junction.

The importance of the Pekola conductance function $\gamma(T)$ is that it is always a *linear* function of temperature, at high enough temperatures. It is predicted to be linear for such systems as solitary junctions, double-junction Coulomb devices, and diffusive wires. An observation of the linearity of this function gives a strong evidence for the Coulomb blockade physics dominating the behavior of the samples. Below we discuss how this type of analysis applies to the samples with insulating wires.

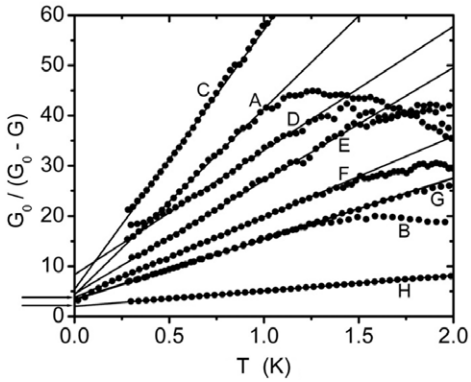

Figure 12. Conductance function $\gamma(T) \equiv G_0/[G_0 - G(T)]$ plotted versus temperature for the set of insulating samples of figure 9(a). The linearity of this function is an indication of the Coulomb blockade phenomenon. The solid lines are fits to the GZ theory (see equations (12) and (13)). Values of the fitting parameter G_0 are such that $G_0^{-1} = 6.14$, 7.14, 7.93, 7.76, 9.78, 9.97, 17.33, and 26.10 kΩ, respectively for the samples A through H. The corresponding normal resistances of the wires are $R_N = 6.43$, 7.54, 8.25, 8.35, 10.33, 10.50, 18.05, and 32.46 kΩ. The range of the offsets, calculated from the GZ theory (the coefficient A of equation (13)) is shown by the horizontal arrows on the left. It is in a qualitative agreement with the actually observed offset values. The lengths of the wires A through H were 46, 45, 140, 105, 140, 49, 120, and 86 nm.

In figure 12 we plot Pekola conductance functions for the insulating samples of figure 9(a). The predicted linearity of the function $\gamma(T)$ is indeed found for all insulating samples, confirming that Coulomb blockade plays a key role in the observed insulating behavior. The parameter G_0 was adjusted to produce the best linearity of these $\gamma(T)$ curves. It turns out that the thus obtained high temperature limit conductance of these samples, G_0, is in good agreement with the normal state conductance R_N^{-1} obtained by direct resistance measurements (see the values listed in the caption to figure 12). Figure 13 presents the values of G_0 plotted versus the inverse normal resistance. It is clear that the results are close to the ideal behavior. In other words, the values of the conductance obtained by linearizing Pekola functions satisfy reasonably well the expected relation $G_0 = R_N^{-1}$.

The offset of the $\gamma(T)$ curves, when extrapolated to zero temperature, should be larger than zero. The arrows in figure 12 show the expected range of the offsets A, calculated using equation (13). The normalized high temperature conductance was taken as $g_0 = R_K/R_N$. The range of slopes is in a semi-quantitative agreement with the experiment.

At higher temperatures ($T > 1$ K) some samples showed a deviation from the linear behavior. Since in all samples the nanowire is connected to the leads, which are superconducting, the observed deviation from the linearity can be attributed to

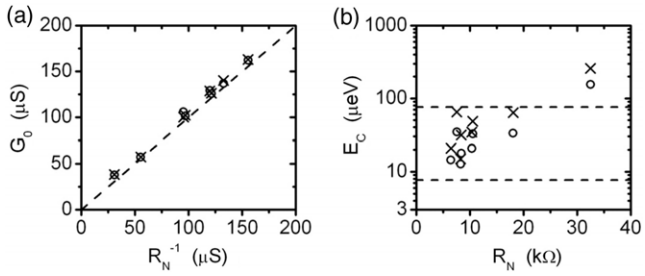

Figure 13. Values of G_0, extracted from the GZ theory fits, plotted versus R_N^{-1}. The crosses (×) represent the G_0 values chosen to provide the best linear behavior of the $\gamma(T)$ curves of figure 12. The open circles (○) represent the G_0 values obtained from voltage-dependent nonlinear measurements, as described by Bollinger *et al* [54]. The dashed line represents the expected theoretical dependence $G_0 = R_N^{-1}$. (b) The crosses represent the charging energies obtained from the slopes B of the linear regions of the $\gamma(T)$ plots in figure 12, using the Golubev–Zaikin formula $E_C = 9k_B/B$. The circles (○) represent E_C values obtained from the voltage-dependent nonlinear measurements, as described in [54]. The two horizontal dashed lines show the range of the charging energies E_C estimated for the given geometry of the electrodes connected to the wire. The uncertainty occurs due to the fact that the exact location of the Coulomb 'horizon' is unknown for these samples.

a suppression of the superconducting proximity effect in the segments of the wire adjacent to the leads. The analysis of those regions is beyond the scope of our discussion here.

Finally, the slope B of the linear regions on the $\gamma(T)$ plots is related to the charging energy of the samples, as $E_C = 9k_B/B$. Thus obtained charging energies for samples A through H are plotted in figure 13. They are compared to the range of charging energies roughly estimated from the geometry of the samples. The range of the estimated charging energies is shown by the two horizontal dashed lines (figure 13). The uncertainty occurs due to the fact that the exact location of the Coulomb 'horizon' is unknown for these samples. Most of the experimental points lie within the region between the two dashed lines, as expected [54].

12. Conclusions

Suspended molecular templates have been used for the fabrication of nanowires with sub-10 nm diameters. The length of such wires could be made as short as ∼40 nm, thus making them some of the thinnest and shortest wires ever studied. This fabrication method made possible an observation of a dichotomy in the wire behavior. Two qualitatively different regimes have been observed, which can be characterized as 'superconducting' and 'insulating'. The geometric characteristics of the wire and correspondingly its normal resistance determine to which group the wire belongs. An approximate condition was found for 'short' wires, i.e. those shorter than ∼200 nm (which is an empirical length threshold). The condition is that wires with the normal resistance satisfying $R_N < R_C \approx h/4e^2$ behave as 'true' superconductors and wires with $R_N > R_C \approx h/4e^2$ showed a behavior that can be considered weakly insulating (i.e. the resistance was increasing with decreasing temperature). These observations suggest a quantum phase transition of superconductor–insulator type.

The TAPS theory was applied to describe $R(T)$ curves and showed a very good agreement with the measurements, for short wires with $R_N < R_C$. These wires behave as 'true superconductors' and should approach zero resistance at temperature is pushed to zero. It appears also that the S-type wire $R(T)$ curves agree with some of the QPS-based theories [45, 109].

Deviations from the TAPS theory have been observed on wires with $R_N > R_C$. Among these wires, the short ones ($L < 200$ nm) exhibit an insulating behavior, as already mentioned above. Such wires are described by models involving weak Coulomb blockade, with an additional assumption that superconductivity is completely suppressed in them, possibly due to proliferation QPS. The $R(T)$ curves of longer wires showed a decrease of the resistance with cooling, even those which satisfy $R_N > R_C$. They were fitted with the Giordano model, involving quantum tunneling of phase slips. Good fits were obtained for the majority of tested long wires ($L > 200$ nm). These wires can be expected to have a finite resistance at zero temperature, due to quantum phase slippage (N1 type). Thus a clear-cut SIT can only be seen in short wires. Longer wires show a gradual crossover behavior.

The origin of the SIT apparent in the short wires can be explained qualitatively as being due to coupling of QPS to gapless excitations in the environment [11, 13–16], similar to the origin of the Schmid–Bulgadaev transition [49–52]. The QPS-free regime can be understood assuming that the QPS are suppressed due to a coupling of the wire condensate to a Caldeira–Leggett type of environment [47, 48, 45]. This environment can be due to a collective effect of the QPS normal cores [54, 45] and plasmons in the leads [44, 45]. In the insulating phase the QPS proliferate and completely suppress superconductivity by their normal cores.

An alternative explanation for the observed superconductor–insulator phase transition can be derived from the presence of local magnetic moments on the surface of wires, possibly occurring due to strong disorder on the oxidized surface. The presence of such moments was suggested by Rogachev *et al* [80]. As the wire diameter becomes smaller, the effective concentration of local magnetic moments increases and, at some point, they can destroy the superconductivity in the wire, due to the well-known Abrikosov–Gor'kov mechanism [39, 81]. This possibility was discussed in [53], and a theoretical analysis of pair-breaking quantum phase transitions in nanowires has been carried out in [104–106]. Further understanding of the SIT can be gained by using microwave techniques [107].

Acknowledgments

The author would like to thank T Aref, M Bae, A Bollinger, M Brenner, R Dinsmore, D Pekker, R Rogachev and M Sahu for critically reading this paper, for valuable suggestions and many useful discussions. This work was supported by the NSF CAREER grant DMR-01-34770 and the DOE grants DEFG02-96ER45434 and DEFG02-91ER45439. Part of the work was carried out in the Frederick Seitz Materials Research

Laboratory Central Facilities, University of Illinois, which is partially supported by the US Department of Energy under grants DE-FG02-07ER46453 and DE-FG02-07ER46471.

References

[1] Graybeal J M 1985 *PhD Thesis* Stanford University
[2] Graybeal G M and Beasley M R 1984 *Phys. Rev.* B **29** 4167
[3] Yazdani A and Kapitulnik A 1995 *Phys. Rev. Lett.* **74** 3037
[4] Turneaure S J, Lemberger T R and Graybeal J M 2000 *Phys. Rev. Lett.* **84** 987
[5] Bollinger A T, Rogachev A, Remeika M and Bezryadin A 2004 *Phys. Rev.* B **69** 180503(R)
[6] Frydman A 2003 *Physica* C **391** 189–195 (and references therein)
[7] Likharev K K 1979 *Rev. Mod. Phys.* **51** 101
[8] Orlando T P and Delin K A 1991 *Foundation of Applied Superconductivity* (Reading, MA: Addison-Wesley)
[9] Skalare A, McGrath W R, Bumble B, LeDuc H G, Burke P J, Verheijen A A, Schoelkopf R J and Prober D E 1996 *Appl. Phys. Lett.* **68** 1558
[10] Semenov A D *et al* 2007 *Supercond. Sci. Technol.* **20** 919
[11] Likharev K K 1986 *Dynamics of Josephson Junctions and Circuits* (New York: Gordon and Breach)
[12] Chen W, Rylyakov A V, Patel V, Lukens J E and Likharev K K 1999 *IEEE Trans. Appl. Supercond.* **9** 3212
[13] Leggett A J 1980 *Prog. Theor. Phys. Suppl.* **69** 80–100
[14] Leggett A J 1978 *J. Physique Coll.* **39** C6 1264
[15] Leggett A J 1987 *Chance and Matter (Les Houches Summer School, Session XLVI, June/August 1986)* ed J Souletie, J Vannimenus and R Stora (Amsterdam: North-Holland) chapter VI
[16] Leggett A J and Garg A 1985 *Phys. Rev. Lett.* **54** 857
[17] Leggett A J, Chakravarty S, Dorsey A T, Fisher M P A, Garg A and Zwerger W 1987 *Rev. Mod. Phys.* **59** 1
[18] Martinis J M, Devoret M H and Clarke J 1987 *Phys. Rev.* B **35** 4682
[19] Makhlin Y, Schön G and Shnirman A 2001 *Rev. Mod. Phys.* **73** 357
[20] Averin D V 1998 *Solid State Commun.* **105** 659
[21] Nakamura Y, Pashkin Y A and Tsai J S 1999 *Nature* **398** 786
[22] Orlando T P, Mooij J E, Tian L, Van der Wal C H, Levitov L, Lloyd S and Mazo J J 1999 *Phys. Rev.* B **60** 15398
[23] Mooij J E and Harmans C J P M 2005 *New J. Phys.* **7** 219
[24] Mooij J E and Nazaron Y V 2006 *Nat. Phys.* **2** 169
[25] Giordano N 1988 *Phys. Rev. Lett.* **61** 2137
Giordano N and Schuler E R 1988 *Phys. Rev. Lett.* **63** 2417
Giordano N 1990 *Phys. Rev.* B **41** 6350
Giordano N 1991 *Phys. Rev.* B **43** 160
Giordano N 1994 *Physica* B **203** 460
[26] Bezryadin A, Lau C N and Tinkham M 2000 *Nature* **404** 971
[27] Lau C N, Markovic N, Bockrath M, Bezryadin A and Tinkham M 2001 *Phys. Rev. Lett.* **87** 217003
[28] Zaikin A D, Golubev D S, van Otterlo A and Zimányi G T 1997 *Phys. Rev. Lett.* **78** 1552
[29] Matveev K A, Larkin A I and Glazman L I 2002 *Phys. Rev. Lett.* **89** 096802
[30] Refael G, Demler E, Oreg Y and Fisher D S 2003 *Phys. Rev.* B **68** 214515
[31] Büchler H P, Geshkenbein V B and Blatter G 2004 *Phys. Rev. Lett.* **92** 067007
[32] Kociak M, Kasumov A Yu, Gueron S, Reulet B, Khodos I I, Gorbatov Yu B, Volkov V T, Vaccarini L and Bouchiat H 2001 *Phys. Rev. Lett.* **86** 2416
[33] Smith R A, Handy B S and Ambegaokar V 2001 *Phys. Rev.* B **63** 094513
[34] Xiong P, Herzog A V and Dynes R C 1997 *Phys. Rev. Lett.* **78** 927
[35] Miyazaki H, Takahide Y, Kanda A and Ootuka Y 2002 *Phys. Rev. Lett.* **89** 197001
[36] Little W A 1967 *Phys. Rev.* **156** 396
[37] Langer J S and Ambegaokar V 1967 *Phys. Rev.* **164** 498
[38] McCumber D E and Halperin B I 1970 *Phys. Rev.* B **1** 1054
[39] Tinkham M 1996 *Introduction to Superconductivity* 2nd edn (New York: McGraw-Hill)
[40] Lukens J E, Warburton R J and Webb W W 1970 *Phys. Rev. Lett.* **25** 1180
[41] Newbower R S, Beasley M R and Tinkham M 1972 *Phys. Rev.* B **5** 864
[42] Sharifi F, Herzog A V and Dynes R C 1993 *Phys. Rev. Lett.* **71** 428
[43] Büchler H P, Geshkenbein V B and Blatter G 2004 *Phys. Rev. Lett.* **92** 067007
[44] Khlebnikov S and Pryadko L P 2005 *Phys. Rev. Lett.* **95** 107007
[45] Meidan D, Oreg Y and Refael G 2007 *Phys. Rev. Lett.* **98** 187001
[46] Werner P and Troyer M 2005 *Phys. Rev. Lett.* **95** 060201
[47] Leggett A J 1980 *Prog. Theor. Phys. Suppl.* **69** 80
[48] Caldeira A O and Leggett A J 1981 *Phys. Rev. Lett.* **46** 211
[49] Chakravarty S 1982 *Phys. Rev. Lett.* **49** 681
[50] Schmid A 1983 *Phys. Rev. Lett.* **51** 1506
[51] Bulgadaev S A 1984 *JETP Lett.* **39** 315
[52] Penttilä J S, Parts Ü, Hakonen P J, Paalanen M A and Sonin E B 1999 *Phys. Rev. Lett.* **82** 1004
[53] Bollinger A T, Dinsmore R C III, Rogachev A and Bezryadin A 2007 *Preprint* cond-mat/0707.4532v1
[54] Bollinger A T, Rogachev A and Bezryadin A 2006 *Europhys. Lett.* **76** 505
[55] Zgirski M, Riikonen K P, Touboltsev V and Arutyunov K 2005 *Nano Lett.* **5** 1029
[56] Altomare F, Chang A M, Melloch M R, Hong Y and Tu C W 2006 *Phys. Rev. Lett.* **97** 017001
[57] Golubev D S and Zaikin A D 2001 *Phys. Rev.* B **64** 014504
[58] Zgirski M and Arutyunov K Y 2007 *Phys. Rev.* B **75** 172509
[59] Rogachev A, Bollinger A T and Bezryadin A 2005 *Phys. Rev. Lett.* **94** 017004
[60] Rogachev A and Bezryadin A 2003 *Appl. Phys. Lett.* **83** 512
[61] Zhang Y and Dai H 2000 *Appl. Phys. Lett.* **77** 3015
[62] Kelly K F, Chiang I W, Michelson E T, Hauge R H, Margrave J L, Wang X, Scuseria G E, Radoff C and Halas N J 1999 *Chem. Phys. Lett.* **313** 445
[63] Hopkins D *et al* 2005 *Science* **308** 1762
[64] Johansson A *et al* 2005 *Phys. Rev. Lett.* **95** 116805
[65] Bezryadin A and Dekker C 1997 *J. Vac. Sci. Technol.* B **15** 793
[66] Bollinger A T 2005 *PhD Thesis* University of Illinois at Urbana-Champaign
[67] BLP-1.9, purchased from www.minicircuits.com
[68] Little W A 1967 *Phys. Rev.* **156** 396
[69] Little W A 1964 *Phys. Rev.* **134** A1416
[70] Ferrell R A 1964 *Phys. Rev. Lett.* **13** 330
[71] Rice T M 1965 *Phys. Rev.* **140** A1889
[72] Mermin N D and Wagner H 1966 *Phys. Rev. Lett.* **17** 1133
[73] Langer J S and Ambegaokar V 1967 *Phys. Rev.* **164** 498
[74] McCumber D E and Halperin B I 1970 *Phys. Rev.* B **1** 1054
[75] Werthamer N R 1963 *Phys. Rev.* **132** 663
Tewordt L 1965 *Phys. Rev.* **137** A1745
[76] Lukens J E, Warburton R J and Webb W W 1970 *Phys. Rev. Lett.* **25** 1180
[77] Zharov A, Lopatin A, Koshelev A E and Vinokur V M 2007 *Phys. Rev. Lett.* **98** 197005
[78] Pekker D, Bezryadin A, Hopkins D S and Goldbart P M 2005 *Phys. Rev.* B **72** 104517
[79] Chu S L, Bollinger A T and Bezryadin A 2004 *Phys. Rev.* B **70** 214506

[80] Rogachev A, Wei T-C, Pekker D, Bollinger A T, Goldbart P M and Bezryadin A 2006 *Phys. Rev. Lett.* **97** 137001
[81] De Gennes P G 1966 *Superconductivity of Metals and Alloys* (New York: Benjamin)
[82] Tinkham M and Lau C N 2002 *Appl. Phys. Lett.* **80** 2946
[83] Graybeal J M, Mankiewich P M, Dynes R C and Beasley M R 1987 *Phys. Rev. Lett.* **59** 2697
[84] Tucker J R and Halperin B I 1971 *Phys. Rev.* B **3** 3768
[85] Chang Y 1994 *Phys. Rev.* B **54** 9436
[86] Markovic N, Lau C N and Tinkham M 2003 *Physica* C **387** 44
[87] Mohr P J and Taylor B N 2005 *Rev. Mod. Phys.* **77** 1
[88] Nazarov Yu V 1999 *Phys. Rev. Lett.* **82** 1245
[89] Golubev D S and Zaikin A D 2001 *Phys. Rev. Lett.* **86** 4887
[90] Panyukov S V and Zaikin A D 1991 *Phys. Rev. Lett.* **67** 3168
[91] Beckmann D, Weber H B and von Löhneysen H 2004 *Phys. Rev.* B **70** 033407
[92] Joyez P *et al* 1997 *Phys. Rev. Lett.* **79** 1349
[93] Joyez P and Esteve D 1997 *Phys. Rev.* B **56** 1848
[94] Pekola J P, Hirvi K P, Kauppinen J P and Paalanen M A 1994 *Phys. Rev. Lett.* **73** 2903
[95] Averin D V and Likharev K K 1991 *Mesoscopic Phenomena in Solids* ed B L Altshuler, P A Lee and R A Webb (Amsterdam: Elsevier) p 173
[96] Geerligs L J, Anderegg V F, Van Der Jeugd C A, Romijn J and Mooij J E 1989 *Europhys. Lett.* **10** 79
[97] Delsing P, Likharev K K, Kuzmin L S and Claeson T 1989 *Phys. Rev. Lett.* **63** 1180
[98] Cleland A N, Schmidt J M and Clarke J 1990 *Phys. Rev. Lett.* **64** 1565
[99] Wahlgren P, Delsing P and Haviland D B 1995 *Phys. Rev.* B **52** 2293
Wahlgren P 1995 *Licentiate Thesis* Chalmers University of Technology, unpublished
[100] Kauppinen J P and Pekola J P 1996 *Phys. Rev. Lett.* **77** 3889
[101] Ingold G L and Nazarov Yu V 1992 *Single Charge Tunneling, Coulomb Blockade Phenomena in Nanostructures* ed H Grabert and M H Devoret (New York: Plenum) p 21
[102] Devoret M H, Esteve D, Grabert H, Ingold G L, Pothier H and Urbina C 1990 *Phys. Rev. Lett.* **64** 1824
[103] Delsing P, Likharev K K, Kuzmin L S and Claeson T 1989 *Phys. Rev. Lett.* **63** 1180
[104] Lopatin A V, Shah N and Vinokur V M 2005 *Phys. Rev. Lett.* **94** 037003
[105] Shah N and Lopatin A V 2007 *Phys. Rev.* B **76** 094511
[106] del Maestro A, Rosenow B, Shah N and Sachdev S 2007 *Preprint* 0708.0687
[107] Manucharyan V E, Boaknin E, Metcalfe M, Vijay R, Siddiqi I and Devoret M 2007 *Phys. Rev.* B **76** 014524
[108] Aderson P W and Dayem A H 1964 *Phys. Rev. Lett.* **13** 195
[109] Khlebnikov S 2007 *Preprint* cond-mat.supr-con/0709.1820v1